Applicability of Laser-Induced Desorption Quadruple Mass Spectrometry (LID-QMS) for the Determination of Local Deuterium Retention

Reinier Zoomers

June 2013

Supervisors:
Dr. Pedro Zeijlmans van Emmichoven
Rianne ‘t Hoen M.Sc.

DIFFER
Dutch Institute for
Fundamental Energy Research

Universiteit Utrecht

Abstract

Laser-induced desorption quadruple mass spectrometry (LID-QMS) is under development in the target exchange and analysis chamber of MAGNUM-PSI. Research to the applicability of LID-QMS as a diagnostic to determine local deuterium inventories is conducted.

It is concluded that LID-QMS can only be used without calibration with thermal desorption spectroscopy (TDS) for the analysis of standard tungsten samples without created damage when the fluence achieved with Pilot-PSI is known and $\leq 3 \cdot 10^{26} m^{-2}$. Assumptions about the trap energy and trap density in tungsten are necessary for the desorption area determination. These assumptions are validated with TMAP7 simulations for samples and exposures used in this work. Uncertainties arising from assumptions on the trapping depth are included in the error analysis. When using different exposure conditions it is necessary to cross calibrate against TDS to re-validate assumption made. No influence of LID-QMS on TDS profiles is observed. Inconsistencies observed are indicated to be due to irregularities in surface modifications probably arising from irregularities during plasma exposures. This statement is supported by optical microscopy pictures. A trend of increasing deuterium retention for increasing bias voltage is observed. Desorption from high energy traps with LID-QMS seems to be impossible. This is shown by comparing two damaged targets with known trap properties: for both the sample analyzed with LID-QMS and TDS and the sample only analyzed with TDS the high energy traps are completely filled when fitting TDS profiles with TMAP7.

Contents

Abstract 2
1. Introduction 5
1.1 Research goal 6
2. Theory 7
2.1 Behaviour of hydrogen in tungsten 7
2.1.1 Implantation 8
2.1.2 Diffusion 8
2.1.3 Desorption 8
2.2 Surface heating processes LID-QMS 9
3. Experimental setup and procedures 11
3.1 Linear plasma generator device Pilot-PSI 11
3.2 Laser-induced desorption quadruple mass spectrometry 12
3.2.1 Measurement procedure 13
3.2.2 QMS measurement 13
3.2.3 Spot size determination 15
3.3 Thermal desorption spectroscopy 17
3.4 TMAP simulations 17
4. Experiments 19
4.1 Series 1: Check calibration with comparison between LID-QMS and TDS 20
4.2 Series 2: Bias influence on LID-QMS and total deuterium retention 20
4.3 Series 3: Check reproducibility LID-QMS and the influence of high energy traps 20
4.4 Computational experiments 21
5. Results 22
5.1. Desorption area determination 22
5.2 LID QMS Results 24
5.3 TDS Results 29
5.4 Optical Microscope and SEM Results 31
5.5 TDS Simulations 34
6. Discussion 37
6. 1 Plasma exposures 37
6.2 Desorption area determination 37
6.3 LID-QMS measurements 38
6.4 TDS measurements 38

6.5 Optical microscope and SEM results 39
6.6 TDS simulations 39
7. Conclusion 41
7.1 Recommendations for further research 42
Appendices 43
A1. Plasma fluence 43
A2. TDS profiles 44
A3. Optical microscope and SEM pictures 45
A4. TMAP7 simulation TDS profiles 48
A5. TMAP input files 51
A5.1 Enclosure input 51
A5.2 Thermal input 52
A5.3 Diffusion input 52
A5.4 TDS desorption simulation 52
A5.5 LID desorption simulation 55
References 58

1. Introduction

Energy supply is becoming one of the most important and in the long term problematic issues of our basic needs. The energy supply by fossil fuels is limited, while energy demand is increasing every year. Another problem is Greenhouse gas emission and the impact these gasses have on the environment. An example of a Greenhouse gas is carbon dioxide. It is important to investigate alternative energy resources. Fusion energy is a potential major supplier of energy in the future.

Nuclear fusion is not to be confused with nuclear fission, the splitting of an atom into smaller nuclei. The only similarity is the fact that both are nuclear processes. The risks involved in fission are the radioactive reaction products with a long halftime and the risk of a chain reaction, the uncontrolled reaction which takes place when for example cooling fails. These risks are not present with nuclear fusion.

Nuclear fusion is the energy source of the sun. Hydrogen fuses to helium in a four step process, delivering energy we notice every day in the form of light and heat. The process takes place at extremely high pressure and particle density, and at a temperature of $\sim 15 \cdot 10^6 K$. The energy generating fusion reaction in a reactor is related to the fusion reaction at the surface of the sun. Two hydrogen isotopes fuse: tritium and deuterium (see formula (1)).

$$D + T \rightarrow {}^4He(3{,}5\ MeV) + n(14.1\ MeV) \qquad \textbf{(1)}$$

The reaction products are helium and a highly energetic neutron. The reaction fuel is available in almost unlimited amounts. Deuterium can be extracted from seawater and is a stable hydrogen isotope. Tritium, a radioactive hydrogen isotope, is not available in nature and will have to be produced on site. To produce tritium a lithium blanket will be constructed around the burn chamber. Tritium will be produced in the reaction between the produced energetic neutrons and lithium [1], and will react with deuterium. The only radioactive material involved is tritium, which has a low half-life time and is used in the fusion reaction. The only risk concerning tritium is possible retention in the reactor vessel before it is used in the fusion reaction. No chain reaction can take place since the fuel distribution can be stopped at any time.

Since the pressure and particle density at the surface of the sun cannot be achieved in a reactor, fusion should take place at extremely high temperatures ($\sim 150 \cdot 10^6 K$). At this temperature the gaseous behavior is dominated by charged particles (plasma state). The plasma state is one of the four fundamental states (among solid, liquid and gas). By heating a gas molecules or atoms can get ionized. With ionization the number of electrons is increased or decreased, producing charged particles [2]. The plasma state is reached when the gaseous behavior is dominated by these charged particles. A plasma is responsive to electromagnetic fields due to the presence of charged particles.

In a fusion TOKAMAK reactor the electrically charged plasma is contained by a toroidal and a poloidal magnetic field. The toroidal field is created using superconducting magnetic coils, the poloidal magnetic field is created by sending a current through the plasma. At the moment a TOKAMAK fusion reactor (ITER) is being build and should be ready for operation in 2020 in the south of France.

The geometry of the magnetic field is designed such that only a small part of the inner surface of the tokamak is in direct contact with the plasma, the divertor. The divertor will be used to reduce the impurity content of the plasma, to remove helium ash and to extract heat. The divertor must withstand significant particle fluxes ($\sim 10^{24}\ m^{-2}\ s^{-1}$) and heat loads ($\sim 10\ MW\ m^{-2}$). Under these conditions the divertor surface can be damaged by a variety of processes such as physical sputtering and hydrogen retention. Dissociation, recombination and redeposition and the formation of blisters play an important role in hydrogen retention. Hydrogen retention is problematic when the hydrogen isotope tritium is retained. Tritium is radioactive and therefore a maximum amount of tritium of $700\ g$ [3] is set to be allowed to be retained in the wall. Due to the extreme conditions in a fusion reactor the material range for plasma facing components is limited. Beryllium is the material of choice for the first wall. In the original design a divertor target made of carbon fibre-reinforced carbon composite (CFC) with a tungsten baffle was implemented to be replaced only in the D-T operation phase by a full W divertor. Due to cost considerations, the feasibility of installing W from the beginning is under consideration [4].

1.1 Research goal

In this work deuterium retention in tungsten, the candidate-material for the ITER divertor, is investigated, and more specifically the possibility to measure local deuterium retention. Hydrogen has three isotopes: protium (the most frequent available isotope), deuterium and tritium. Nuclear Reaction Analysis (NRA) is a method available to measure local deuterium retention. A new diagnostic under development at DIFFER in Nieuwegein is laser induced desorption quadruple mass spectrometry (LID-QMS). The diagnostic is installed in the Target Exchange and Analysis Chamber (TEAC) of MAGNUM-PSI.

The aim of the present work is to show whether LID-QMS can be used to determine local deuterium retention and to check whether absolute calibration is possible. The influence of LID-QMS on TDS profiles is considered. Also the possibility to measure local deuterium retention immediate after plasma exposure in MAGNUM-PSI is investigated.

To be able to do this solid knowledge of the principles involved is required. To test retention targets will be exposed to a deuterium plasma in Pilot-PSI and in MAGNUM-PSI. Due to the radioactivity of tritium, research possibilities with tritium are limited. Deuterium is used instead of the cheaper hydrogen because hydrogen can already be present at the surface of targets in the form of water. It is important to be able to make a clear distinction between implanted deuterium and hydrogen already present before plasma exposures. In Pilot- and MAGN UM-PSI particle fluxes and heat loads comparable to those at the ITER divertor can be achieved, making the machine suitable for plasma exposures. The radial deuterium retention will be measured by LID-QMS. Thermal desorption spectroscopy (TDS) will be used to perform a cross calibration and check the absolute calibration of LID-QMS.

In this thesis first a theoretical introduction will be given. All the used diagnostics will be discussed in the experimental setup. After that the executed experiments and the results will be discussed, finished by a discussion and a conclusion.

2. Theory

In order to understand the results of the measurements, background information on the behavior of deuterium in tungsten will be provided. To truly understand the results a distinction will be made between deuterium retention in and deuterium desorption from tungsten. With LID-QMS the desorption process is initiated by heating the surface. The mechanisms necessary to understand material heating will be discussed in this section as well.

2.1 Behaviour of hydrogen in tungsten

Deuterium retention, and subsequent desorption by either TDS or LID-QMS is determined by several processes. The number of particles implanted in a material depends on the solubility of a material and the particle influx. The movement of particles through a material is determined by the diffusivity and recombination and dissociation processes at the surface of a material determine the release rate. The combination of these properties and processes determine the behaviour of hydrogen isotopes in tungsten. Retention is also influenced by material modification such as blister formation which can be the effect of plasma irradiation. The inner surface of blister is covered by deuterium atoms and deuterium is dissolved in molecular form inside blisters.
In the theoretical part of this work the main focus will be on diffusion processes and the release processes, since these play an essential role in hydrogen desorption. Implantation will be touched upon, but no details will be given.

Materials are divided in endothermic and exothermic materials. Tungsten in endothermic for deuterium molecules as displayed in figure 1. For exothermic materials it is energetically favourable for particles to be in solution. Tungsten is exothermic for deuterium atoms. In figure 1 the potential energy diagram of tungsten is shown [5]. In this figure E_S is the solubility activation energy, E_T is the trapping energy and E_D is the diffusion barrier. In our experiments deuterium is implanted in atomic form. The different energy levels play a role in diffusion. Diffusion processes will be discussed in section 2.1.2.

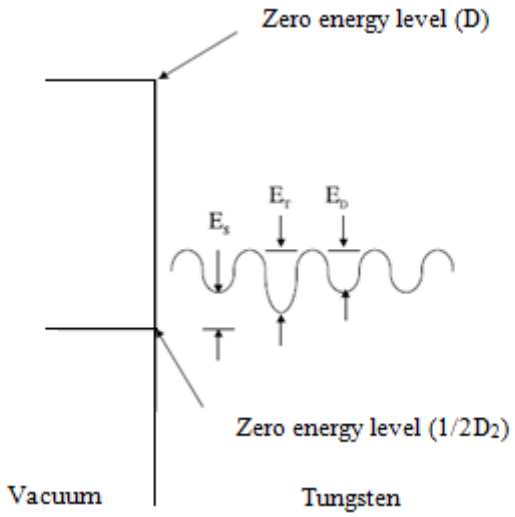

figure 1

The potential energy diagram of tungsten for deuterium. Tungsten is endothermic for molecular deuterium and exothermic for atomic deuterium.

2.1.1 Implantation

Deuterium is implanted when a deuterium atom enters the surface and is trapped in the implantation zone. The implantation zone is the implantation range of incident deuterium atoms. Deuterium implantation is influenced by two processes [5]:

1. Diffusion: Deuterium atoms diffuse from the implantation zone into the material where they get trapped.
2. Blister formation: The material is saturated by deuterium retention. Deuterium dissolves at defects, for example vacancies or voids, forming blisters. In blisters the deuterium can be trapped in atomic and molecular form [6][7].

2.1.2 Diffusion

The movement of deuterium atoms through a material is described by diffusion processes. For diffusion several energy levels are of importance (see figure 1). The diffusion energy barrier E_D is the required energy to move in between two natural sites. The trap energy of a trap site is given by E_T. E_T is the difference between the energy level of a solution site (E_s) and the energy level of a trap site plus the diffusion energy barrier (E_D).

Every material has natural trap sites. Beside natural trap sites with low trap energy and density, additional trap sites with other trap energies can be created in a material. It is energetically favorable for particles to be at the lowest energy level, and thus to be trapped in the trap with the highest trap energy. When a particle is trapped at a low energy level the required energy for detrapping is high. Creating additional trap sites can be a side effect of plasma irradiation (for example blister formation), or it can be done deliberately by heavy ion implantation [8]. In the second case it is possible to implement a known amount of additional trapping sites [8]. In blisters deuterium will be trapped in atomic and molecular form. To leave the material, the deuterium first has to dissociate, move to the surface and recombine again at the surface. The energy required for this extra dissociation process leads to the increased trap energy of blisters. The diffusion equation, equation (2), consists of the diffusion coefficient D_0, basically the jump frequency – jump distance product, and an exponential factor representing the jump probability:

$$D = D_0 Exp[\frac{-E_D}{k_b T}] \qquad (2)$$

E_D is the diffusion energy barrier, k_b is the Boltzmann constant and T is the temperature.

2.1.3 Desorption

At an interface, pressure equilibrium is always sought. Due to deuterium implantation in the near surface regime a pressure difference originates between the surface and its surrounding. If pressure equilibrium is reached dissociation at the surface exactly matches recombination at the surface. When in vacuum, the pressure difference between the enclosure of the sample and the sample surface causes deuterium to recombine at the surface and to desorb from the surface. Because a deuterium atom can also recombine with a hydrogen atoms masses 3 (HD) and 4 (D2) will be monitored in all measurements. A minimum energy is required for detrapping. With LID-QMS this

energy is delivered by heating the surface with a laser beam. Processes involved in surface heating are discussed in the next section. The release rate is given by [5]:

$$Release\ rate = K_R C^2 \quad (3)$$

In formula (3) K_r is the recombination rate coefficient and C is the deuterium concentration close to the surface [5]. A high release rate contributes to a low overall concentration throughout the sample due to rapid deuterium release. A low release rate has the opposite effect.

It was shown by Causey et al [9] that the release rate of deuterium from tungsten was not limited by the recombination coefficient, and is therefore limited by diffusion processes. Similar conclusions about release rate limitations are reported by Haasz et al [10].

2.2 Surface heating processes LID-QMS

To desorb deuterium with LID-QMS the tungsten surface is heated by a laser beam. The heating of a surface and the temperature increase of a surface under laser irradiation is dependent on three different processes:

1. Reflection of the laser beam from the surface
2. Absorption of the laser energy by the material
3. Conduction of the heat through the material (heat diffusion)

The incoming light of the laser is partly reflected from the sample surface, resulting in a loss of incoming energy. If the roughness of the surface is small compared to the wavelength of the laser used, reflection is governed by the Fresnel equations [11]. Assuming a perpendicular income of the laser beam with respect to the surface gives a reflection coefficient of $R{\sim}50\ \%$ in vacuum for the laser used in this work.

Deuterium desorption significantly increases due to heating of the surface. With LID-QMS the surface is locally heated. The heat is absorbed by the material. The Lambert Beer-law describes the absorption in terms of the properties of the concerning material. For tungsten the light is absorbed in the first tens of nanometers [12].

Heat is absorbed in a small part of the surface. After absorption the heat diffuses through the material causing a temperature increase of the material, both in lateral direction and in depth. Therefore diffusion of heat through the material is of great importance for LID-QMS. For a better understanding the heat transfer in a solid is considered. Heat transfer in a solid of a finite thickness can be calculated using a semi-infinite solid configuration. This configuration can be used as long as the penetration depth into the solid is sufficiently small. This means that the heat will only penetrate a short distance into the material compared to the thickness of the material [13]. The radial and depth temperature changes over time due to heat diffusion through the material are given by formula (4) [14].

$$T(r,z,t) = T_0 + \int_0^\infty d\lambda \left(\frac{I}{2K\lambda} J[0, r\lambda] J[1, \alpha\lambda] \right. \quad (4)$$

$$\left. * \left(e^{-z\lambda} Erfc \left[\frac{z}{\sqrt{\frac{\pi K t}{\rho c}}} - \sqrt{\frac{Kt}{\rho c}} \lambda \right] - e^{z\lambda} Erfc \left[\frac{z}{\sqrt{\frac{\pi K t}{\rho c}}} + \sqrt{\frac{Kt}{\rho c}} \lambda \right] \right) \right)$$

where $K = 177\, Wm^{-1}K^{-1}$, $c = 134\, Jkg^{-1}K^{-1}$ and $\rho = 19300\, kgm^{-3}$ are respectively the thermal conductivity, specific heat and density of tungsten [15]. The radial position and the depth are given by r and z and the time is give by t. I is the incident laser energy flux and J is a Bessel funtion. The constants are assumed to be independent of temperature. When $z, r = 0$ the surface temperature can be approximated by [16]:

$$T = T_0 + \frac{2}{\sqrt{\pi}} \frac{I\sqrt{t}}{\sqrt{Kc\rho}} \quad (5)$$

This approximation is very important in the process of LID-QMS measurements. It will be used to estimate laser conditions required to reach desired maximum surface temperatures.

3. Experimental setup and procedures

In this section the different experimental setups used during this work will be described. In the process of determining the applicability of LID-QMS samples have to be exposed to a deuterium plasma first. With LID-QMS you want to measure the implanted deuterium profile. Therefore it is important to have a clear distinction between implanted hydrogen and naturally present hydrogen. Exposures are performed with the linear plasma generator device Pilot-PSI. After implantation LID-QMS measurements are executed followed by thermal-desorption spectroscopy measurements (TDS). The results are simulated with TMAP7. A brief introduction of the used setups will be given in the described order with relevant parameters.

3.1 Linear plasma generator device Pilot-PSI

The Pilot-PSI linear plasma generator is displayed in figure 2. The device is used for deuterium implantation by plasma irradiation. The device produces ITER divertor-like plasma parameters and is therefore suitable to study plasma surface interactions for divertor materials. The cascaded arc plasma source produces high density low electron temperature plasma (see figure 2). Plasma parameters are in the range $T_e \sim 1-5\ eV, n_e \sim (0.1-10)\times 10^{20}\ m^{-3}$.

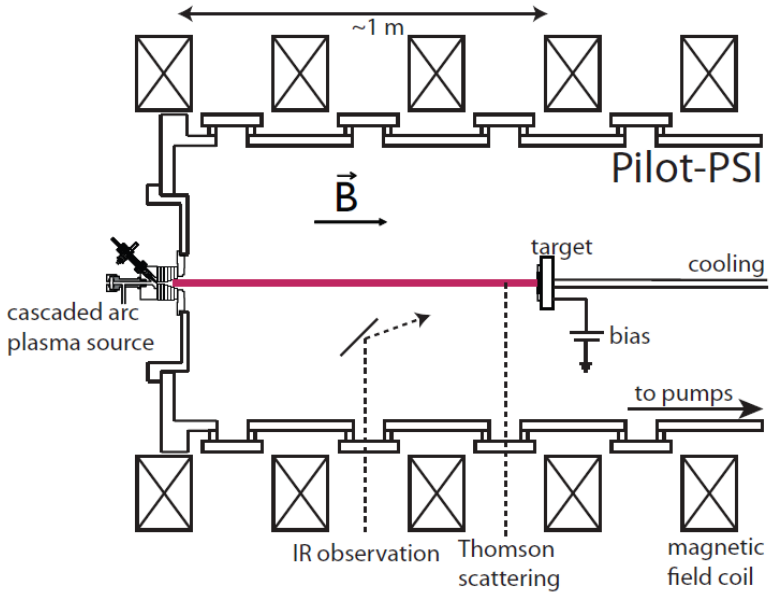

figure 2

Schematic drawing of the linear plasma generator device Pilot-PSI. Optical emission spectroscopy (OES) is not shown in the figure but is installed at the first window from the left, next to the IR camera.

The magnetic field confines the plasma beam directing it to the installed target. Several diagnostics can be installed at the device. The plasma parameters are measured with a Thomson scattering system close to the target [17]. Surface temperatures can be measured with two different calibrated infrared cameras, the FLIR SC7000 or the FLIR A645. To measure plasma impurities and check the source performance the plasma light is observed using optical emission spectroscopy (OES).

3.2 Laser-induced desorption quadruple mass spectrometry

The LID-QMS setup is installed in the TEAC of MAGNUM-PSI, and is schematically shown in figure 3. The laser used for LID-QMS is a Nd:YAG laser, with a wavelength of $1064\ nm$. The laser is situated in the laser room and connected to the TEAC by a high transmission fiber. The maximum output energy of the laser is $60\ J$ and the exposure time ranges from $0.1 - 20\ ms$. The fiber connecting the laser with the TEAC can handle a maximum power of $20\ kW$. When entering the TEAC the laser beam is focused to a spot on the target by a set of achromatized lenses. Losses of laser energy consist of transmission losses in the fiber ($\sim 25\ \%$), reflection on the TEAC window ($\sim 8\ \%$) and reflection from the target ($\sim 50\ \%$) (see section 2.2). Losses in the fiber and due to reflection from the TEAC window are experimentally determined by placing a joule meter in the TEAC. The total energy loss from laser to target can now be calculated to be $\sim 65\ \%$.

The targets are installed in the TEAC on the multi-target holder, on which three targets can be mounted. This target holder can be moved, tilted and rotated, making it easy to align the target with the laser beam. The focus of the laser does not significantly change in between measurements because the target is moved instead of the laser beam. The released deuterium is measured with a quadruple mass spectrometer (QMS) (HiQuad WMG 700). Mass 3 (HD) and mass4 (D2) are measured and summed to get the total amount of deuterium desorbed. In order to identify the signal and to stay within the operating range of the QMS it is critical to perform the measurement in vacuum. A threshold for deuterium implanted must be reached in order to be able to measure a LID-QMS signal. This will be further discussed in the experimental results.

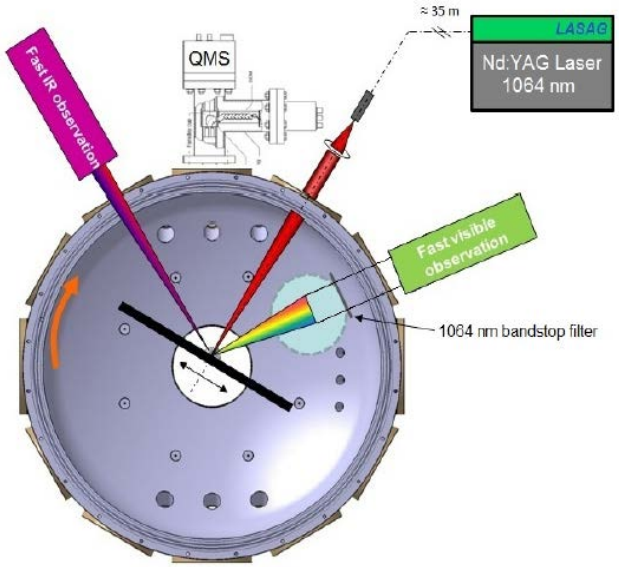

figure 3
Schematic drawing of the LID-QMS setup in the Target Exchange and Analysis Chamber (TEAC) of MAGNUM-PSI.

3.2.1 Measurement procedure

The schematic process of a LID-QMS measurement is depicted in figure 4. After the measurement procedure it takes around 5 minutes for the vessel pressure to return to its original value. When the pressure is stabilized another measurement can be performed. The maximum surface temperature can be approximated by formula (5). This approximation is used to determine the pulse conditions, the pulse energy in combination with pulse duration, necessary to reach the desired surface temperature. The measurement procedure is repeated three times at each location to make sure approximately all the deuterium is desorbed. As shown by Bas Hensen and other earlier measurements $\sim 90\ \%$ of the deuterium is desorbed in the first shot and therefore almost complete desorption in three shots is assumed [12][30]. A typical LID-QMS measurement is plotted in figure 6.

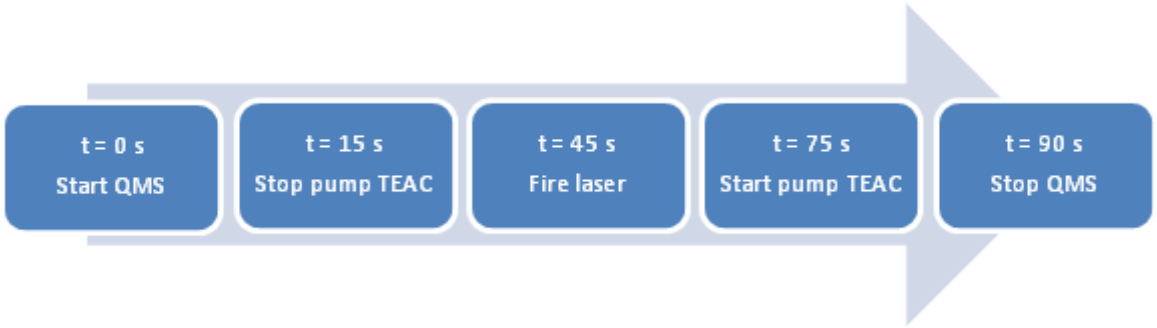

figure 4
The schematic representation of a LID-QMS measurement.

3.2.2 QMS measurement

The deuterium retained from the exposed samples is measured using a quadruple mass spectrometer (QMS). A range of masses is measured during each cycle. The cycle duration of the QMS is approximately $0{,}9\ s$. The relevant masses measured are mass 3 (HD) and 4 (D2). Masses 19 (HDO) and 20 (D2O) do not exceed background levels and are therefore neglected.

Figure 5 shows the schematic of a quadruple mass spectrometer [18]. Incoming atoms or molecules are ionized by the electron impact ionizer. After ionization the ions pass the quadruple mass filter. The quadruple mass filter consists of four cylindrical rods set parallel to each other. The quadruple is responsible for filtering ions by their mass to charge ratio. The opposing pairs of rods are electrically connected. A radio frequency voltage is applied between the pairs of rods, and a direct current voltage can be superimposed on this radio frequency voltage. The applied voltages affect the trajectory of ions. By tweaking the voltage ions of a certain mass-to-charge ratio can be selected. Therefore specific ions can be measured by the detector. Ions with other mass-to-charge ratios will not reach the detector. By continuously changing the applied voltage a range of mass-to-charge ratios can be measured making it possible to get signals of atoms with different masses. A photomultiplier tube is connected to the detector to be able to convert the signal to counts. The number of counts is expressed in ion current.

The output signal of the QMS is given in ion current (A) of the individual masses. The error in the QMS signal is determined using Poisson statistics and ranges from $4{,}0\ \% - 12{,}0\ \%$ for respectively the maximum ion current measurable and the background ion current (see figure 7). This is the statistical standard deviation using Poisson statistics for the number of counts [19]. Since a margin is

taken in reaching the measuring limit of the QMS the uncertainty of the QMS is set to be $8{,}0\ \%$. A calibration is performed to transform the ion current into atoms/s. In order to do the calibration the background signal of deuterium and hydrogen needs to be determined. After closing the valve to the turbo pump a linear increase of the ion current is observed for all monitored masses (see figure 6). The increase in ion current is correlated with the increase in the vessel pressure. This pressure increase can be caused by small leaks in the TEAC or material release from the TEAC walls. The calibration is performed by repeating the procedure with a calibrated deuterium leak connected to the TEAC. Both the background and calibration measurements are now fitted. The fit represents $\Delta I/\Delta t$ (in A/s). The resulting calibrated signal is obtained by subtracting the background measurement from the calibration measurement. The flow rate in mol/sec of the calibrated deuterium leak is known. Using the Avogadro constant N_A this can be converted in dN/dt (in molecules per second). The calibration factor C is now given by:

$$C = \frac{\frac{dN}{dt}}{\frac{\Delta I}{\Delta t}} \qquad (6)$$

The calibration factor C is given in molecules/A. With this calibration factor known, measured QMS signals can be converted to deuterium molecules retained. Since the background signal is not constant over time the calibration needs to be done again every measurement. When performing an actual measurement a step increase in ion current is observed. A typical measurement is displayed in figure 6. The slope of the deuterium signal changes after the laser shot. Deuterium desorption is determined by analyzing the step in ion current [20]. The change of the slope is not completely understood. Possible influences could be the spreading of the desorbed deuterium over the TEAC volume (very short timescale) and the sticking of deuterium to the vessel. When pumping the vessel down a significant decrease in ion current over time is observed showing outgassing of the vessel. The pressure increase caused by the LID-QMS measurement provides a possibility for the opposite effect, the sticking of deuterium to the vessel.

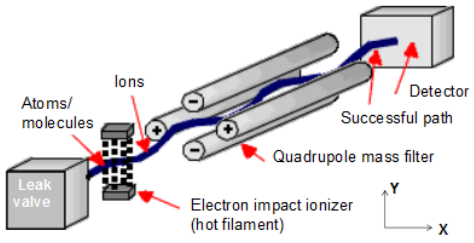

figure 5

Schematic of the quadruple mass spectrometer. Atoms and molecules are ionized by the electron impact ionizer. The quadruple mass filter filters out ions with a specific mass-to-charge ratio, which are measured with the detector. A photomultiplier is inserted to be able to measure the number of counts of the signal.

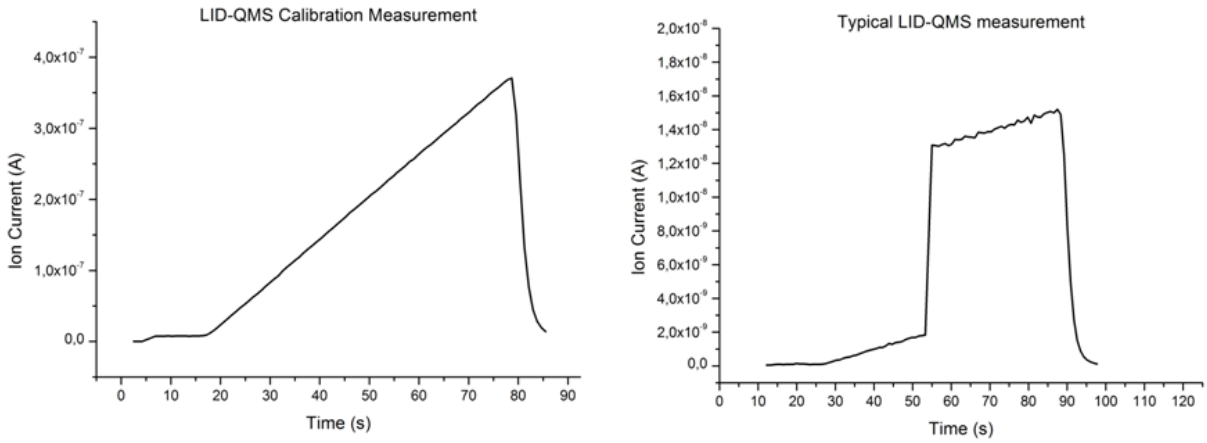

figure 6

LID-QMS calibration measurement (left) and typical LID-QMS measurement (right). In the left graph a step increase in ion current is observed when the shot is performed, showing deuterium desorption. The linear increase in ion current before the actual shot represents the background signal.

3.2.3 Spot size determination

LID-QMS is designed to get information about the local retention of hydrogen isotopes. To compare the local retention to overall retention a comparison with TDS has to be made. Therefore the LID-QMS signal needs to be expressed in molecules/m^2. Because of the high impact of the spot size on the quantification of LID-QMS the spot size is estimated using three different procedures:

1. Empirical laser beam analysis
2. Analysis fast infrared camera
3. Modeling of surface temperature profile

The result of the spot size determination experiment is described in the experimental section since knowledge on the spot size is essential to be able to perform the actual experiments.

3.2.3.1 Empirical laser beam analysis

When performing LID-QMS measurements the laser beam is focused on the target to a minimum laser beam diameter. Due to internal reflections in the fiber and a lack of knowledge about the lenses used it is impossible to calculate the beam diameter. To determine the laser beam diameter a diaphragm and a power meter are installed in the TEAC, located respectively just in front of and at the target position. The aperture of the diaphragm is decreased over different laser shots and the energy arriving at the power meter is measured (see figure 7).

In general a laser beam has a Gaussian beam profile. The internal reflections in the fibre should transform this into a homogeneous profile [16]. Figure 7 does not show a constant profile however, since the transmitted energy as function of diaphragm diameter is not a step function. The laser beam diameter is estimated to be between $2 - 3\ mm$ considering figure 7. This information gives an estimation of the surface directly irradiated by the laser beam.

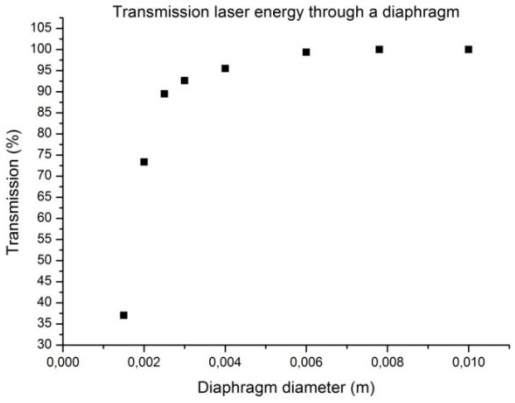

figure 7

Transmission of the laser energy as function of diaphragm diameter.

3.2.3.2 Analysis fast infrared camera

The sample surface temperature can be determined using the fast infrared camera. A 2 dimensional temperature profile is produced. Surface temperature IR measurements can therefore be used reproduce the radial temperature profile of the laser spots.

3.2.3.3 Modeling of surface temperature profile

Solving formula (4) provides the temperature depth profile and the radial temperature profile of a surface. The resulting temperature profile is plotted in a contour plot in figure 8. Since desorption will be validated to be $\sim 100\ \%$ with TMAP7 simulations for surface temperatures $T > 1000\ K$, the highest temperature plotted is $T = 1500\ K$ to produce a clear plot. The maximum surface temperature $T \sim 2300\ K$ is therefore not plotted. The pulse duration is set to $3\ ms$ and the laser irradiated area is assumed to have a diameter of $d = 2{,}5\ mm$. This contour plot will later be compared with the IR camera image to check for inconsistencies.

The temperature dependent spot size is now determined. The laser spot is defined. For determining the desorption area, the temperature dependent laser spot has to be corrected for the desorption dependence on surface temperature. This process will be discussed in section 4.

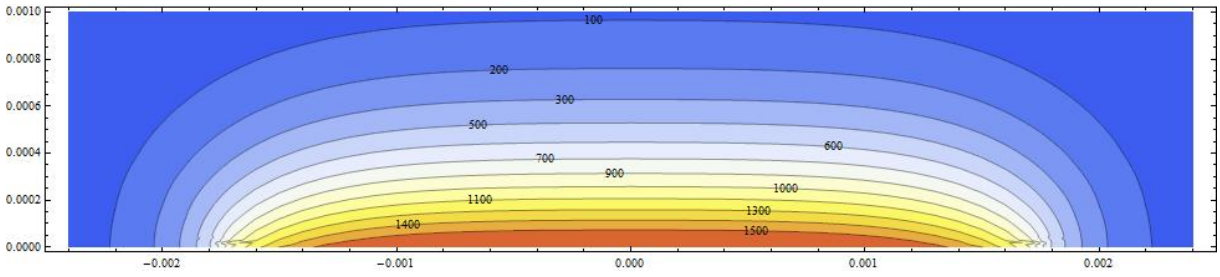

figure 8

Theoretical contour plot of the temperature profile of a tungsten sample under laser irradiation. On the x-axis the radial position on the sample surface is plotted, on the y-axis the depth of the sample is plotted.

3.3 Thermal desorption spectroscopy

Thermal desorption spectroscopy (TDS) is used to determine the deuterium inventory in samples [21]. With TDS measurements, a ceramic heater is used to heat the target with a linear ramping speed. In this work a ramping speed of $1\ K/s$ is used for all the measurements. Different peak locations can be determined due to this slow heating rate. The samples are heated to a temperature of $1273\ K$ and are kept at this temperature for ten minutes to make sure all deuterium is desorbed. The temperature is then linearly ramped down to $500\ K$, at which temperature the heater is turned off. A selection of masses is measured with a Balzers QMA125 QMS. Of specific interest for deuterium retention are the masses 3 (HD) and 4 (D2) signals measured in the residual gas in the TDS chamber. Masses 19 (HDO) and 20 (D2O) do not exceed the background values and are therefore neglected. The measurements are calibrated using a calibrated D2-leak.

3.4 TMAP simulations

In this work the behavior of trapped deuterium in tungsten, diffusion through the sample and desorption from the surface, is simulated with the 1D Tritium Migration Analysis Program 7 (TMAP7) [22]. The version used is an update from the original program developed to analyze tritium related safety issues. TMAP7 is used to get a better understanding of the obtained TDS profiles and deuterium desorption by LID-QMS, and to get agreement between simulations and experiments. TMAP7 is used to simulate both TDS and LID-QMS measurements.

TMAP7 simulates deuterium behavior in tungsten. The behavior is simulated by solving the diffusion equations. In TMAP7 a distinction is made between diffusivity in bulk tungsten and at the tungsten surface. The equations are solved for a specific deuterium implantation profile, and for a specific temperature development of the sample. The output of the simulations is given by the particle flux leaving the surface, the temperature and the trapped and mobile deuterium concentrations. More information about the input files and the possibilities of TMAP7 is given in appendix A5.

TMAP7 will be used to fit the TDS signals and to determine the implantation profile of the samples. With LID-QMS simulations more information and knowledge about the deuterium desorption percentage dependency on surface temperature and deuterium implantation depth will be obtained. Deuterium desorption during TDS and LID-QMS is dependent on five different properties:

1. Surface temperature
2. Trap depth
3. Trap densities
4. Trap energies
5. Fill factor of the traps

On the timescale of TDS these properties determine the peak locations. Deuterium trapped in low energy traps is released at low temperatures, deuterium trapped in high energy traps is released at high temperatures. During TDS measurements all the deuterium is eventually released, because the sample is kept at high temperatures during a long timescale. The sample is kept at the maximum temperature of $T = 1273\ K$ for ten minutes.

The short timescale and extreme heating rate of LID-QMS might limit the desorption of deuterium. Therefore the described properties influence the percentage of trapped deuterium that can be desorbed by LID-QMS.

To fit the simulations to the TDS measurements the surface temperature, trap depth, trap density and trap energy can be changed. More information about TMAP7 is given in appendix A5.

4. Experiments

In this section the experiments executed are described. Preliminary measurements are done which are not shown in the results. For these measurements samples are exposed to a deuterium plasma with MAGNUM-PSI, and analyzed afterwards with LID-QMS. Deuterium retention was not sufficient to result in a LID-QMS signal. Also the deuterium background level is too high directly after exposures to use the QMS. It takes two days of pumping before the background level is low enough to measure. This limits the possibilities for instant LID-QMS measurements directly after exposures with MAGNUM-PSI. Since Pilot-PSI can reach significant higher fluences then MAGNUM-PSI during comparable time frames since the cooling down time of the magnets is significantly shorter, further exposures are done with Pilot-PSI. For low temperature plasma exposures (T_{max}~$500\ K$) the radial deuterium retention profile is shown to represent the plasma flux profile [23]. Since samples with radial retention profiles provide the perfect opportunity to check the possibility to measure local deuterium retention all exposures are done at or below this maximal surface temperature.

The heated area by the laser is determined like described in section 3.2.3. The spot size determination is repeated for every measurement series to check the consistency of the setup. Desorption is $< 100\ \%$ for lower surface temperatures. So not al the deuterium is desorbed from the heated area, since part of this area does not reach sufficient surface temperatures. Desorption percentage dependency on surface temperature will be simulated with TMAP7. The desorption area is determined by correcting the heated area for desorption dependency on surface temperature. Part of the heated area is excluded from the desorption area. This part excluded corrects for the part where 100% desorption is theoretically not possible. A temperature limit is now determined where this correction theoretically results in 100% desorption. The surface area corresponding to this temperature is set to be the desorption area.

The measurements are divided and executes in three different series:

- Series 1: Check calibration with comparison between LID-QMS and TDS
    - -40V bias exposed samples (sample R01.1 and R02.1)
- Series 2: Bias influence on LID-QMS and total deuterium retention
    - bias scan (sample R06 – R12)
- Series 3: Check reproducibility LID-QMS and the influence of high energy traps
    - -40V bias exposed samples (sample K01 – K04, FF12 and FF15)

LID-QMS analysis is executed three times per location to make sure approximately all the deuterium is desorbed, as discussed in the experimental setup. Measurements are performed in random order to be able to check for the inter-spot influence. Laser settings are kept constant for all measurement series. The settings for the laser energy, pulse duration, frequency and burst number are tabulated in table 1. The burst number represents the number of pulses fired. These setting lead to a surface temperature T~$2300\ K$.

table 1

Information about the laser settings used for the LID-QMS measurements. The laser settings are kept constant over the different measurement series. The settings lead to a surface temperature $T \sim 2300K$.

Parameter	Value
Laser energy (J)	39,6
Pulse duration (ms)	3
Frequency (Hz)	2
Burst number	1

4.1 Series 1: Check calibration with comparison between LID-QMS and TDS

In series 1 one pair of samples is exposed to deuterium plasma with Pilot-PSI. Similar fluences are achieved. The main goal is see whether desorption by LID-QMS shows results similar to the TDS signal and shows a profile similar to the plasma profile. Only one of the two samples is analyzed with LID-QMS. Both samples are analyzed with TDS. This is done to be able to make a comparison between a sample analyzed with LID-QMS and a sample not irradiated by the laser, and to check whether laser irradiation influences the TDS profile. Optical microscopy pictures are made to check for possible blister formation.

4.2 Series 2: Bias influence on LID-QMS and total deuterium retention

Series 2 consists of a bias scan. Samples are exposed with biases ranging from floating (no bias) to -40V bias. The bias difference between the different samples is 10V. The comparison between LID-QMS and TDS is made to check if the measured signals show similar results to the total deuterium desorption signal, and to check whether biasing influences LID-QMS . Another incentive is to check the influence of bias voltage on total deuterium retention. All the targets are exposed to similar fluences. The -20V, -30V and -40V biased targets are analyzed with LID-QMS, and all targets are analyzed with TDS. To check surface blister formation SEM and optical microscope pictures are made.

4.3 Series 3: Check reproducibility LID-QMS and the influence of high energy traps

In series 3 six samples are exposed in pairs to deuterium plasma with Pilot-PSI with -40V bias. Four samples are standard polished tungsten samples. Two samples are damaged with high energy heavy ions to deliberately create artificial traps in the material. The goal of series 3 is to check the reproducibility of series 1 and 2. The damaged targets are included to check the influence of higher trap energies on deuterium desorption by LID-QMS. High energy traps are created in these samples [8]. One sample of each pair is analyzed with LID-QMS. All are analyzed with TDS to be able to make the comparison and to check the influence of laser irradiation. Surface pictures are made to check for possible blister formation.

4.4 Computational experiments

Simulations are done for all samples measured. They are specifically referred to here as a specific measurement series. The computational experiments are divided in two different sets of simulations:

1. Fitting the TDS profiles with TMAP7 to obtain information about the implantation profile.
2. Determination desorption dependency on surface temperature and hydrogen implantation depth.

4.4.1 TDS simulations

In section 3.4 the different properties influencing deuterium desorption were discussed. These properties can be changed in the TMAP7 input files to get a fit of the TDS profiles.
Some uncertainties have to be taken into account when interpreting the results from TMAP7 simulations and drawing conclusions using these simulations. The main disadvantage of these simulations is the non-uniqueness of obtained results. Similar fits can be made with different input values for trap energies, concentrations and implantation depths. This uncertainty is minimized by using best practise values for trap energies and concentrations from literature [8][24][25][26]. The samples used are all samples from the same tungsten role. Therefore trap energies are kept constant over the different measurement series. The trap concentration for the natural traps is kept constant as well, since this is primarily a property of the material. Trap concentrations for possible blisters are not kept constant since this depends on the blister size and blister density and therefore varies per sample due to different plasma irradiation conditions. An order of magnitude estimation for the trapping depth of deuterium trapped in blisters is made: the trapping depth is assumed to be similar to the size of the blister on the surface. The trap energy for deuterium trapped in blisters is kept constant, and the value is checked by comparing it with values found in literature.

For the damaged targets FF12 and FF15 the trap density, depth and energy are known [8]. Therefore these parameters are set and cannot be changed. For standard tungsten samples the traps are assumed to be completely filled up. Trap densities of damaged targets are much higher, significantly more traps are available. Since it is energetically favourable for deuterium atoms to be trapped in the highest energy trap, this trap is assumed to be completely filled. The fill factor of the lower energy traps can be changed to be able to get an optimal fit of the TDS results.

By combining results obtained before in literature and keeping essential parameters constant the uncertainties are minimized, but still have to be kept in mind when using TMAP7 simulations and when using the simulations to conclude on retention properties. It is hard to determine a quantitative uncertainty for TMAP7 results.

4.4.2 LID-QMS simulations

TMAP7 simulations are performed to determine desorption percentage dependency on surface temperature and deuterium implantation depth. Results are used for the desorption area determination, as described before, and to get a better understanding about the workability and applicability of LID-QMS. The LID-QMS simulations will be discussed in combination with the desorption area determination.

5. Results

In this section the results obtained will be presented. Since the desorption area needs to be determined before quantifying the LID-QMS signal the desorption area determination will be discussed first, followed by the different analyses done.

The exposure information of the samples used is displayed in table 2. The fluence is calculated by multiplying the flux with the exposure time. More information on how to calculate the flux and the fluence is provided in appendix A1. The flux is the flux calculated from the maximum Thomson scattering values, and is therefore the flux in the centre of the plasma beam. This results in an overestimation of the averaged flux and fluence over the sample. The maximum flux is used anyway to be able to make a direct comparison during exposures. The flux profile is Gaussian and similar in between measurements (see figure 11 to figure 17). Radial dependent flux profiles are created after the exposures.

table 2

Exposure information of the targets used in this work. The desorbed deuterium is the combined amount of deuterium desorbed by LID-QMS and by TDS. The flux is the flux at the center of the plasma beam.

Sample	Deuterium (m^{-2})	Exposure time (s)	Flux ($m^{-2}s^{-1}$)	Fluence (m^{-2})	Bias (V)
R01.1	6,54E+19	220	1,11E+24	2,45E+26	-40
R02.1	6,24E+19	220	1,34E+24	2,96E+26	-40
R06	5,66E+19	220	1,41E+24	3,09E+26	-10
R07	1,94E+20	300	1,01E+24	3,03E+26	-40
R08	9,35E+19	230	1,31E+24	3,02E+26	-20
R09	2,44E+20	300	1,01E+24	3,02E+26	-30
R12	5,05E+19	200	1,56E+24	3,13E+26	Floating
K01	1,51E+20	240	1,06E+24	2,48E+26	-40
K02	1,23E+20	310	8,31E+23	2,50E+26	-40
K03	1,71E+20	250	1,11E+24	2,82E+26	-40
K04	1,49E+20	200	1,30E+24	2,62E+26	-40
FF12	7,33E+20	310	9,36E+23	3,09E+26	-40
FF15	5,38E+20	320	1.34E+24	3,81E+26	-40

5.1. Desorption area determination

To determine the desorption area first the laser heated area of the surface has to be determined like discussed in section 4. An IR-camera recording of the laser spot is made and analyzed. The radial temperature profile of the laser spot in pixels when the surface has reached its maximum surface temperature is displayed in figure 9. The conversion from pixels to mm is displayed on the right of the figure.

In figure 10 both the theoretical temperature and deuterium implantation depth dependency of desorption are plotted. These plots are obtained by performing LID-QMS simulations with TMAP7.

The results are plotted for trap density $\rho_t = 2 \cdot 10^{-5}$ and $\rho_t = 5 \cdot 10^{-5}$. The natural trap density for the samples used is $\rho_t = 2 \cdot 10^{-5}$. This value is found and checked with values from literature. Simulations with trap density $\rho_t = 5 \cdot 10^{-5}$ are executed to get an indication of the trap density influence.

For the temperature dependence simulations the deuterium implantation depth is set to be $5\ um$. The hydrogen implantation depth dependence is simulated for surface temperature $T = 1500\ K$. Relevant implantation depths for deuterium implantation with Pilot-PSI will be validated in section 5.5 to be up to $40\ um$ for the measurement series executed. In the right part of figure 10 the influence of this implantation depth on desorption is checked. The error margin resulting from the desorption dependency on implantation depth is determined to be $10\ \%$. This error margin will be included in the desorption area determination. For implantation depths achieved in our measurements this is the maximum influence of deep deuterium implantation on the temperature dependence of desorption.

All simulations use trap energy $E_t = 1{,}1\ eV$. This trap energy is comparable to values found in literature. This is an important assumption in the absolute calibration of LID-QMS. It is impossible to perform LID-QMS simulations for high energy traps since the detrapping time is orders of magnitude longer than the measurement time. Due to this high detrapping time it is theoretically impossible to desorb deuterium from high energy traps. Deuterium trapped in blister should be treated differently, since blister are formed on the surface and could be destroyed by the laser beam desorbing the trapped deuterium.

Combining figure 10 and figure 11 the radius of the desorption area is now calculated to be $r = 1{,}3\ mm$ with an error margin of $10\ \%$. The desorption area is defined to match a theoretical desorption of 100%. The radius is constant over the different measurement series.

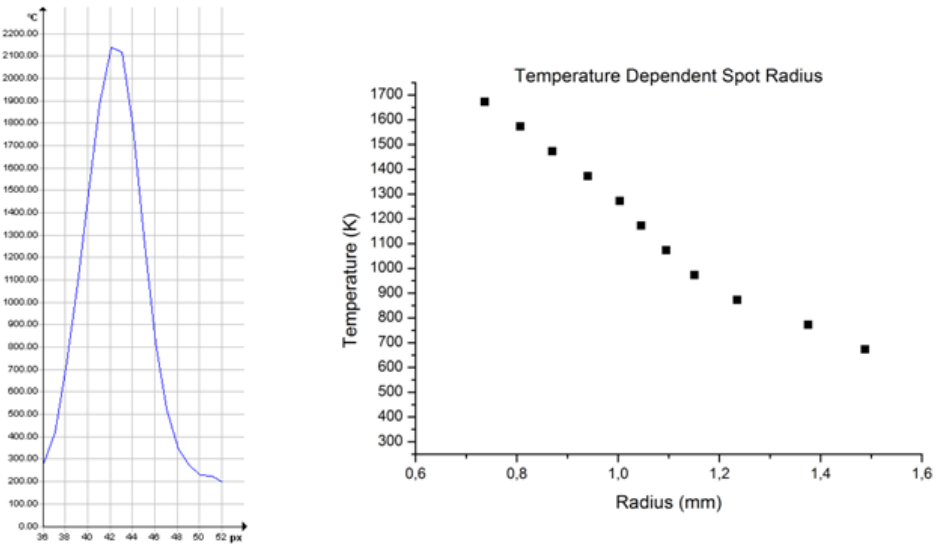

figure 9

Temperature profile of a laser spot on a tungsten sample measured with the IR-camera (left).The temperature dependent spot size in mm is displayed on the right.

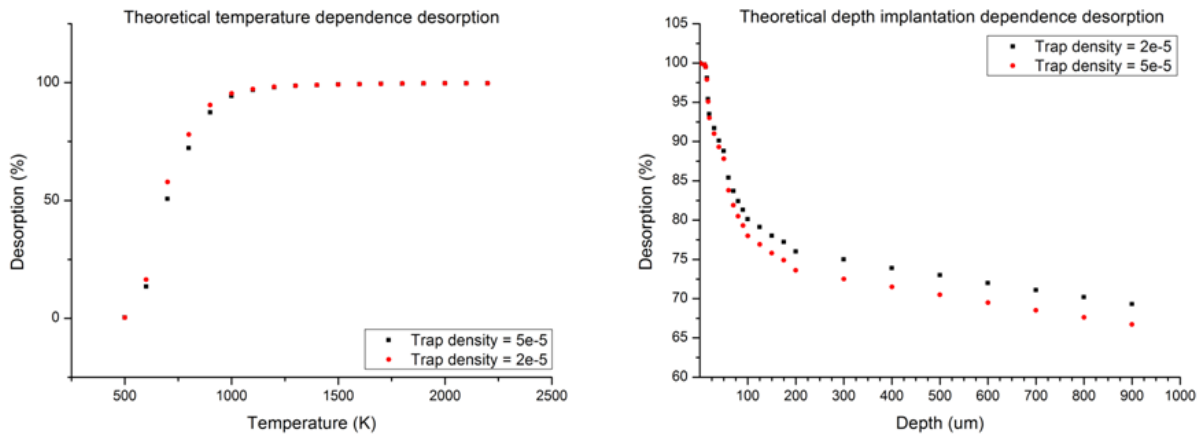

figure 10

At the left the theoretical temperature dependence of desorption is plotted. The hydrogen implantation depth is set to be $5\ um$*. At the right the depth implantation dependence of desorption is plotted. The simulation is executed for a maximum surface temperature of* $T = 1500\ K$*.*

5.2 LID QMS Results

The research goal is to check whether it is possible to measure local deuterium retention without calibration with TDS. LID-QMS is performed on different positions on the target to get a representation of the plasma profile. Because the exposures done are all low temperature exposures the radial retention profile is expected to represent the plasma flux profile [23]. The error in the QMS signal (section 3.2.2: $8\ \%$) and the error in the desorption area determination (section 5.1: $10\ \%$) contribute to the error in the LID-QMS signal. The error is calculated using standard error propagation [19]. The area of the desorption radius is determined in the previous section to be $r = 1{,}3\ mm$. Three measurements per location are executed. On average $\sim 90\%$ of the desorbed deuterium is measured during the first shot. This percentage is consistent with LID-QMS measurements described in literature [12][24]. The third measurement did not show a signal for any of the samples analyzed.

All plots in this section contain the plasma flux profile, the LID-QMS measurements per radial spot (sum of the three shots) and the total deuterium desorption signal. The total deuterium desorption signal is the sum of all LID-QMS measurements and the TDS measurement.

5.2.1 Results series 1: Check calibration with comparison between LID-QMS and TDS

In figure 11 the LID-QMS profile of sample R02.1 reflects the plasma profile. An inter-spot influence in between the spots measured is observed. The desorption areas seem to overlap. This is not true when checking the positions of the different spots in figure 11. One has to keep in mind however that the desorption area is defined such that $100\ \%$ is theoretically possible. Deuterium is desorbed outside the desorption area as well, but this deuterium compensates for areas with desorption $< 100\%$. So even when desorption areas do not overlap still an inter-spot influence can be observed. Therefore the heated areas of the spots should not overlap instead of the desorption areas. The second and fourth spot from the left do not represent the plasma profile and are located below the overall trend. LID-QMS measurements result in signals comparable to the total deuterium desorption

indicating complete desorption and indicating proper absolute calibration. Signals at the edges are below the total desorption signal, signals close the center are above the overall deuterium desorption signal. This is a proper representation of the plasma profile.

5.2.2 Results series 2: Bias influence on LID-QMS and total deuterium retention

Three samples of the bias scan are measured with LID-QMS (-20V, -30V and -40V bias exposed samples). High deuterium retention compared to series 1 is achieved while similar exposure fluences are reached (see table 2). This indicates irregularities during the exposures of series 1 leading to a significant lower deuterium retention. No irregularities are observed with OES. A possible explanation could be a bias malfunction during exposures. Sample R07, R08 and R09 are plotted in figure 12, figure 13 and figure 14 in the order of the bias voltage.

The -20V biased target (figure 12) does not show a radial profile. One LID-QMS measurement is above the total desorption signal, the rest of the measurements are below. LID-QMS signals are comparable to the total deuterium desorption signal.

The -30V biased target (figure 13) does show a radial profile. Three spots are located above the total desorption signal, one below. LID-QMS signals are comparable to the total deuterium desorption signal.

LID-QMS measurements of the -40V biased target (figure 14) seem to be completely random and no radial profile whatsoever is observed. This measurement was the first of series 2, but the results are presented in order of bias voltage. Three signals are located on or above the total desorption signal, two spots are located below the total desorption signal. The second spot from the right is analyzed first. Since the neighboring spots have signals below the total desorption signal only four measurements per target are executed on the other targets to exclude the risk of overlapping heated areas.

Possible effects of high temperature exposures on the retention profile [8] are excluded by doing all exposures at low sample surface temperatures. It is hypothesized that surface modifications by the increased deuterium retention compared to series 1 could result in the inconsistencies observed between the plasma profile and the LID-QMS. Inhomogeneous blister formation or inhomogeneous impurity deposition could influence local deuterium retention or desorption. These inhomogeneous surface modifications would indicate irregularities during plasma exposures. This hypothesis will be checked by analyzing the surfaces by optical microscope and SEM. No bias influence on LID-QMS signals is observed.

5.2.3 Results series 3: Check reproducibility LID-QMS and the influence of high energy traps

The results of the analysis of sample K01 are plotted in figure 15. LID-QMS measurements on different locations over the target represent the plasma profile. The total deuterium desorption signal is within the errormargins of two of the LID-QMS measurements. The measurements at the edge of the target are located below the total desorption signal.

Analysis of sample K04 (figure 17) shows similar phenoma as observed with the analysis of the -20V and -40V biased samples of series 2. The measured LID-QMS signals are partly above, partly at and

partly below the total desorption signal. The hypothesis stated for series 2 will also be checked for this sample by taking optical microscopy surface pictures.

Desorption by LID-QMS from sample FF12 (figure 17) is lower than the total desorption signal. In section 5.1 it is stated that it is theoretically impossible to desorb deuterium trapped in high energy traps with LID-QMS. Analysis of sample FF12 supports this statement. Further insight in the amount of deuterium trapped in high energy traps and therefore in the possible influence on LID-QMS measurements will be obtained in section 4.4.1.

In general LID-QMS measurements on undamaged tungsten targets result in signals comparable to the total deuterium desorption signal. This indicates correct absolute calibration. Radial profiles partly follow the plasma profile and partly not. It is hypothesized that inhomogeneous surface modifications, blister formation or impurity deposition, could influence the radial profile. If this hypothesis is correct one would expect inhomogeneous surface modifications for sample R07, R08 and K04. No inhomogeneous surface modifications are expected for sample R02.1, R09 and K01. The hypothesis will be checked by producing optical microscopy surface pictures.

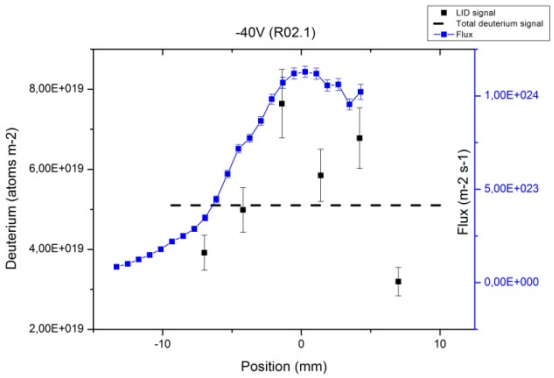

figure 11

Overview plot of the analysis of sample R02.1. The LID-QMS and total desorption results are plotted on the left y-axis, the plasma profile is plotted on the right y-axis. An inter-spot influence is observed. LID-QMS signals are comparable to the total desorption signal.

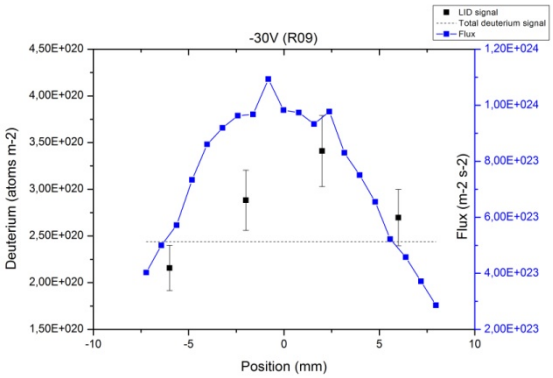

figure 13

Overview plot of the analysis of sample R09. The LID-QMS and total desorption results are plotted on the left y-axis, the plasma profile is plotted at the right y-axis. The LID-QMS results correspond to the exposure plasma profile. LID-QMS signals are comparable to the total desorption signal.

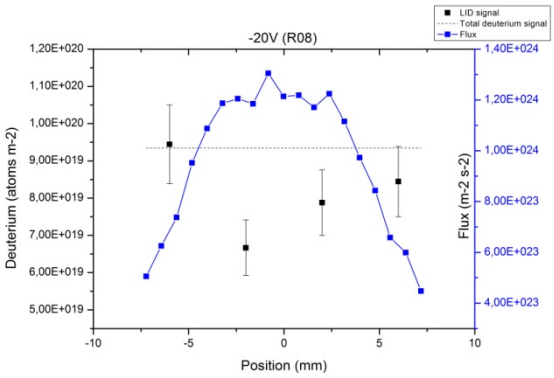

figure 12

Overview plot of the analysis of sample R08. The LID-QMS and total desorption results are plotted on the left y-axis, the plasma profile is plotted at the right y-axis. A discrepancy between the LID-QMS measurements and the plasma profile is observed.

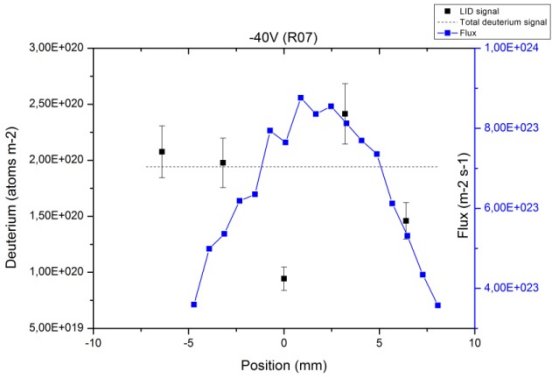

figure 14

Overview plot of the analysis of sample R07. The LID-QMS and total desorption results are plotted on the left y-axis, the plasma profile is plotted at the right y-axis. The plasma profile is not represented by the LID-QMS results. LID-QMS signals are comparable to the total desorption signal.

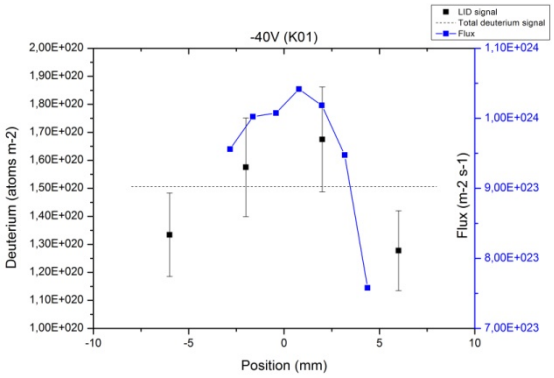

figure 15

Overview plot of the analysis of sample K01. The LID-QMS and total desorption results are plotted on the left y-axis, the plasma profile is plotted at the right y-axis. QMS signals show similarities with the plasma profile.

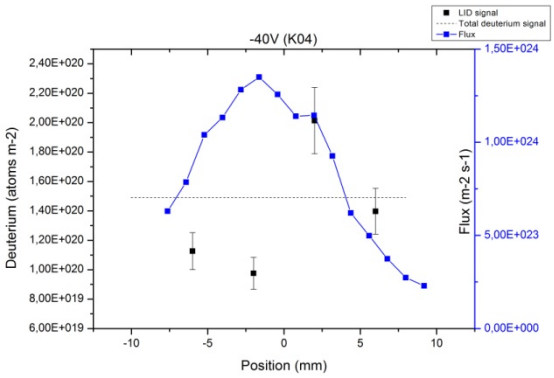

figure 16

Overview plot of the analysis of sample K04. The LID-QMS and total desorption results are plotted on the left y-axis, the plasma profile is plotted at the right y-axis. Similar phenomena resulting in a discrepancy between the plasma profile and the LID-QMS measurements as with the -20V and -40V biased samples are observed.

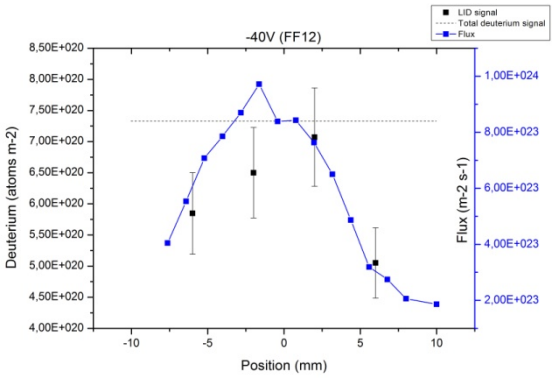

figure 17

Overview plot of the analysis of sample FF12. The LID-QMS and total desorption results are plotted on the left y-axis, the plasma profile is plotted at the right y-axis. LID-QMS signals seem to be shifted to the right compared to the plasma profile. The LID-QMS signals are below the total desorption signal .

5.3 TDS Results

TDS is used to determine the total deuterium inventory in targets. LID-QMS signals are added to get the total deuterium desorption signal. Total deuterium desorption signals of the different samples are presented in table 2. The total desorption signals are implemented in the plots in the previous section. As discussed earlier the samples in series 1 and series 3 are exposed in pairs to check whether the TDS profiles are influenced by LID-QMS measurements. With the bias scan the influence of bias on total deuterium retention is checked by performing TDS measurements.

In figure 18 the TDS profiles of series 1 are plotted. Sample R01.1 is only analyzed with TDS, while sample R02.1 is also analyzed with LID-QMS. Only one peak is observed in both profiles. In section 5.5 this low temperature peak will be validated to be linked to the natural trap energy of tungsten ($E_t = 1{,}1eV$). No influence of LID-QMS is observed in the TDS profile. No new peak or a peak location shift is present.

The TDS results of series 2 used to determine the total deuterium inventory are included in appendix A2. TDS profiles.

In figure 19 the TDS profiles of series 3 are plotted. The samples are exposed in pairs, sample K01 and K04 are analyzed with both LID-QMS and TDS and sample K02 and K03 are only analyzed with TDS. A low and a high temperature peak are observed. The high temperature peak is hypothesized to indicate blister formation. This hypothesis will be checked by making optical microscope and SEM pictures of the surface and by doing TMAP7 simulations. For sample K01 and K02 the high temperature peak exceeds the low temperature peak, for sample K03 and K04 the low temperature peak exceeds the high temperature peak. Like in series 1 no influence of LID-QMS on the TDS profile is observed. The high temperature peaks are hypothesized to be linked to blister formation on the surface. Since LID-QMS signals are comparable to total deuterium desorption signals, deuterium trapped in blister seems to be desorbed despite the high trapping energy. Desorption is caused by the destruction of blisters by the laser beam.

Considering the results of series 3 one would also expect a high energy peak in figure 18. The absence of this peak indicates a non-biased exposure also supporting the low retention seen from table 2 and therefore the possibility of a bias malfunction.

In figure 21 the deuterium retention dependency on bias voltage is plotted for the bias scan executed. All samples are exposed to similar fluences. A large uncertainty comes in here because it is impossible to expose samples to identical fluences. The fluence calculated is the maximum fluence not taking into account the plasma profile. The error in the fluence is estimated to be $\sim 20\%$. Since the fluence is assumed constant this uncertainty cannot directly be plotted. Therefore a horizontal uncertainty of 20% is added to the plot. The uncertainty in the deuterium signal arises from the uncertainty in the QMS signal. This measurement is only used to indicate a trend. In general an increase in deuterium retention is observed for increasing bias. Considering the uncertainties discussed the decrease in retention after the -30V biased target is within the error margin.

The TDS profiles of FF12 and FF15 look similar. This indicates that LID-QMS does not influence TDS profiles. Whether it is possible to desorb deuterium trapped in high energy traps will be discussed in section 5.5.

It is shown that LID-QMS measurements do not influence the TDS deuterium desorption profiles. No peak location shift or a shift in between peaks is observed. Blister formation is indicated by the presence of a high temperature peak in series 2 and 3. TDS results of the samples of series 3 show a differentiation in deuterium retention for samples exposed to similar fluences under similar plasma conditions. This indicates irregularities in the plasma exposures.

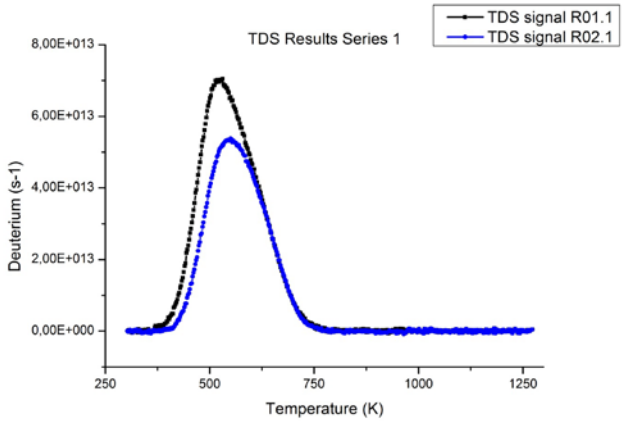

figure 18

TDS results of series 1. Sample R01.1 is only analyzed with TDS, sample R02.1 is analyzed with both TDS and LID-QMS. No influence of LID-QMS on the TDS profile is observed.

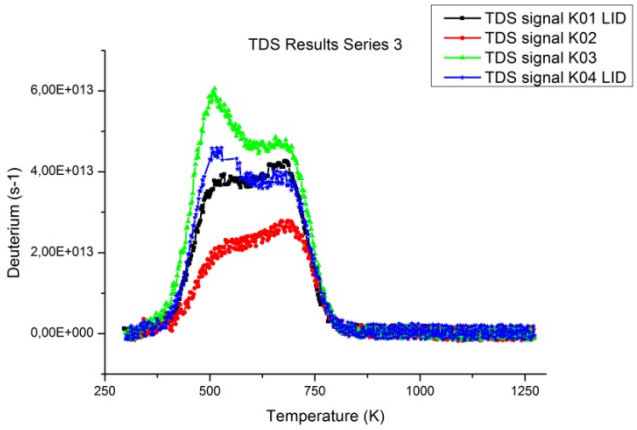

figure 19

TDS results of the standard samples of series 3. Sample K01 and K04 are analyzed with LID-QMS first. No influence of LID-QMS on the TDS profile is observed.

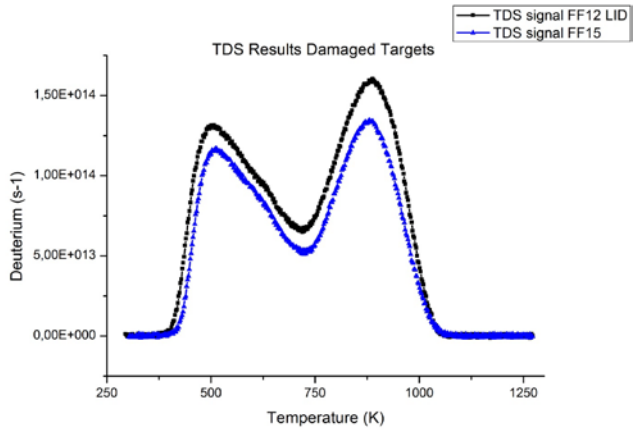

figure 20

TDS results of the damaged targets of series 3. The similar shape of the profiles indicates that LID-QMS does not influence TDS profiles.

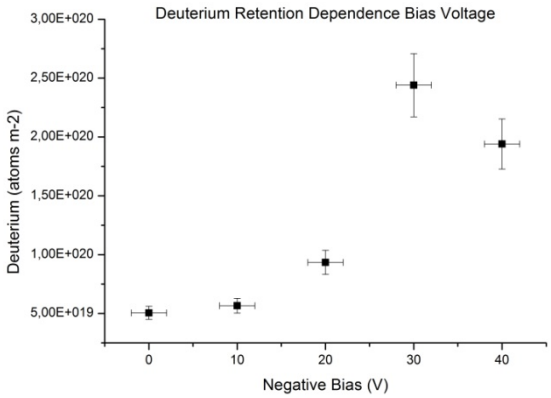

figure 21

Deuterium retention dependency on bias voltage. Increased retention is observed for increased negative bias. A decrease in retention is observed for the -40V biased sample, but this decrease is within the error margin and is therefore not significant.

5.4 Optical Microscope and SEM Results

Inhomogeneous surface modifications are hypothesized to influence the consistency of LID-QMS measurements. High energy peaks were observed in TDS profiles of series 2 and 3, which will later be validated with TMAP7 to be linked to blister formation. Considering TDS results nothing can be said about the possible presence of impurities. Optical microscope pictures are made of all samples analyzed, SEM pictures are made of the bias scan.

In figure 22 surface pictures of sample R01.1 and R02.1 (series 1) are shown. The TDS profiles only show low temperature peaks. High temperature TDS peaks are assumed to be linked to high energy traps. For undamaged tungsten targets high energy traps are linked to blister formation. For damaged targets high temperature peaks originate from the created damage. For sample R01.1 and R02.1 no blister formation is therefore expected. This is verified by figure 22. This supports the

possibility of a bias malfunction during exposures which is also indicated by the total deuterium retention and by the TDS profiles.

In figure 23 blister presence is clearly indicated for the -40V biased sample (R07). White spots on the optical microscope picture presented at the right show the presence of large blisters. When zooming in with SEM blisters on a smaller scale are also observed. An overview of the SEM pictures of the bias scan is attached in appendix A3.

Inhomogeneous surface modifications are shown in figure 24 for the same sample displayed in figure 23 (sample R07). The two pictures are made on similar distances from the center of the plasma beam to minimize flux dependent effects. Therefore one would expect homogeneous blister formation. The opposite effect is observed however. Some impurities are also observed (black spots). This verifies the hypothesis stated in section 5.2 that inhomogeneous surface modifications influence the consistency of LID-QMS measurements. If a desorption area with either relatively high or low blister density is analyzed with LID-QMS this could theoretically result in either a high or a low LID-QMS signal and in a subsequent discrepancy with the plasma profile. Sample R07, R08 and K04 show inconsistencies between LID-QMS measurements and the plasma profile (figure 12, figure 14 and figure 17). By scanning the surfaces indeed inhomogeneous blister formation and impurities are observed. The pictures for sample R08 and K04 are attached in appendix A3. Scanning the rest of the samples by optical microscope did not show inhomogeneous surface modifications at all, corresponding with the fact that the plasma profiles are represented by LID-QMS measurements. The surface pictures of sample R09 are displayed in figure 25, the pictures of sample K01 are attached in the appendix.

In this section it is shown that inconsistencies in LID-QMS measurements can be linked to inhomogeneous surface modifications. It is not clear what causes inhomogeneous surface modifications. They are most likely the result of irregularities during plasma exposures.

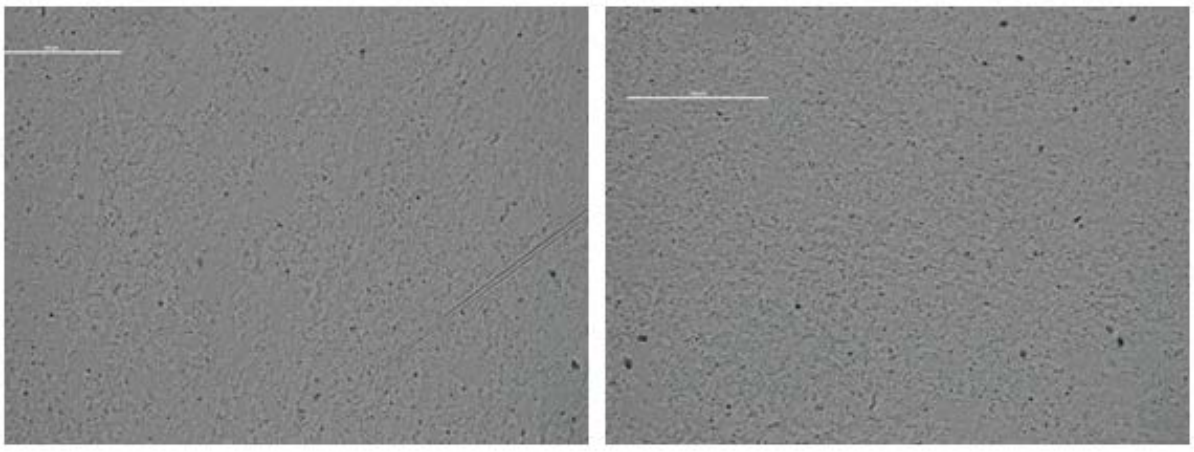

figure 22

Surface picture of sample R01.1 (left) and R02.1 (right) after plasma exposure. No blister formation is observed. This result is conformable with the TDS results.

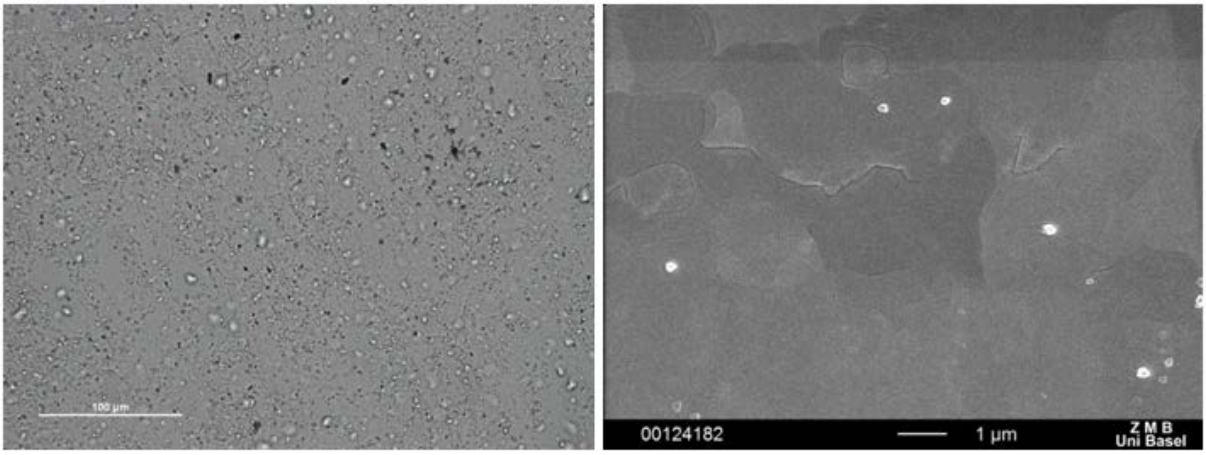

figure 23

Blister formation on the -40V biased sample surface (R07). White spots on the optical microscope picture on the left show blister presence. When zooming in with SEM (right picture) also blisters on a smaller scale are observed.

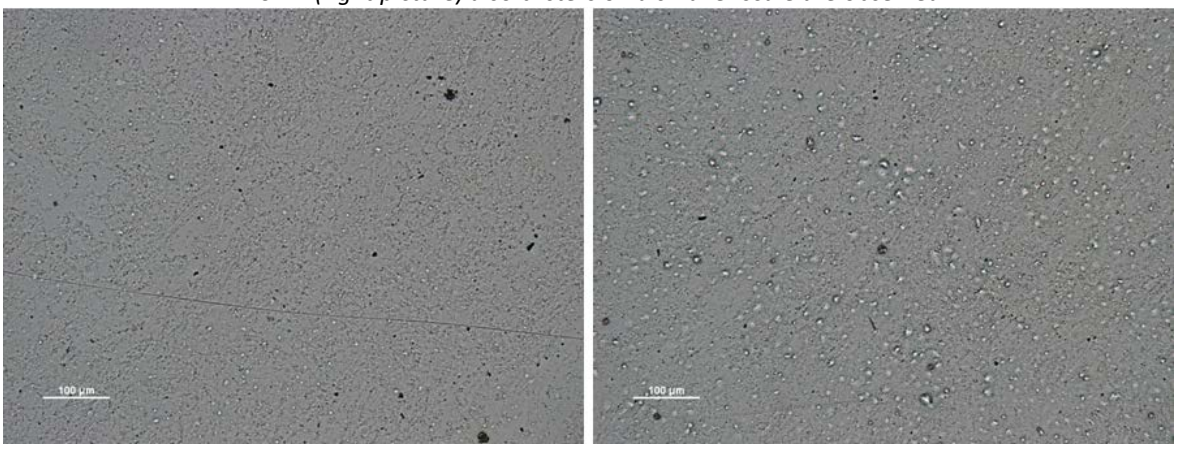

figure 24

Inhomogeneous blister formation on the -40V biased sample surface (R07). Differences in blister formation are observed while considering the plasma flux at the locations of the pictures taken one would expect similar pictures. Impurities are also present.

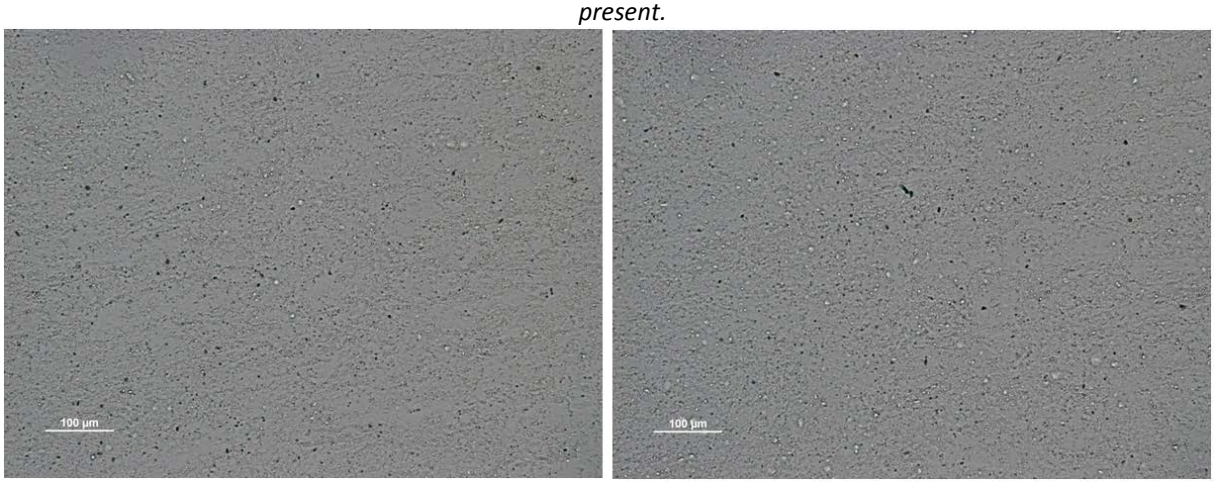

figure 25

Blister formation on the -40V biased sample surface (R09). White spots on the optical microscope pictures show blister presence. Surface modifications seem to be homogenous. The complete sample surface is scanned.

5.5 TDS Simulations

This section is devoted to the simulation of TDS measurements. These simulations reproduce the implantation profile of the exposed samples. The trap concentrations and energies will be deduced. TMAP7 simulations are executed to fit the measured TDS profiles. The natural trap energy for the standard tungsten samples used in series 1, 2 and 3 is $E_{t1} = 1.1\ eV$. Blister present have a trapping energy of $E_{t2} = 1.7eV$. Deuterium trapped in blisters can be desorbed by LID-QMS due to the destruction of blisters by the laser beam. The values for the trap energies are obtained by fitting the TDS profiles starting with values from the range of trap energies found in literature for similar experiments [8][25][26][27]. The same method is followed for the trap density of the natural traps: $\rho_t = 2 \cdot 10^{-5}$. The trap density for blisters is not kept constant during the simulations, since this depends on the blister density and blister size as discussed in section 4.4.1 TDS simulations. The trap density of blisters is significantly higher than the trap density for natural traps for all simulations, since deuterium is trapped in molecular form in blisters. For the blister size an order of magnitude estimation is made from the SEM pictures. This estimation is used for the implantation depth, since blisters are expected to by symmetric.

Fit optimization is now performed by changing the implantation depth of trap 1 and by changing the trap density and, on a very small scale, the implantation depth of trap 2. An example of a TDS profile and the TMAP7 fit to this profile is given in figure 26 for sample K04 (-40V bias series 2). The rest of the TMAP7 fits are attached in appendix A3.

The results of series 1 are displayed in table 3. As already observed in the optical microscope pictures no blisters are formed at the surface. Therefore the trap concentration and trap depth are set to 0 for the high energy traps linked to blister formation. No high energy traps linked to blisters are found. This supports the indication of a bias malfunction during exposures found in the total deuterium retention from the samples, the absence of blisters on optical microscopy pictures and the lack of a high temperature peak in the TDS profiles.

The results of series 2, the bias scan, are displayed in table 4. No high temperature peak is observed for the -10V biased target. This is represented by the input parameters deduced from the fit made.

The results of the standard tungsten samples exposed to -40V bias of series 3 are displayed in table 5. Limited trapping depth of deuterium in the natural trap for sample K04 is observed. This is also represented by the relatively low deuterium retention in this sample.

Computational results of the damaged targets are displayed in table 6. Although both samples are exposed to similar fluences retention in sample FF12 is significantly higher. When comparing the fits obtained with TMAP7 this is represented by lower fill factors of the low energy traps in sample FF15. The high energy traps are completely filled for both samples. This indicates a lack of desorption from high energy traps with LID-QMS, since these traps are still completely filled after LID-QMS measurements are executed. This supports the hypothesis that deuterium trapped in high energy traps cannot be desorbed with LID-QMS.

Since trap energies and densities are kept constant and validated by values found in literature the uncertainties in the simulations are minimized. It is still important to be careful however when drawing solid conclusions based on TMAP7 results. The simulations in this work are primarily executed to verify the assumptions made in the desorption area determination about the deuterium implantation depth and to check variations in implantation depths in between separate similar exposures.

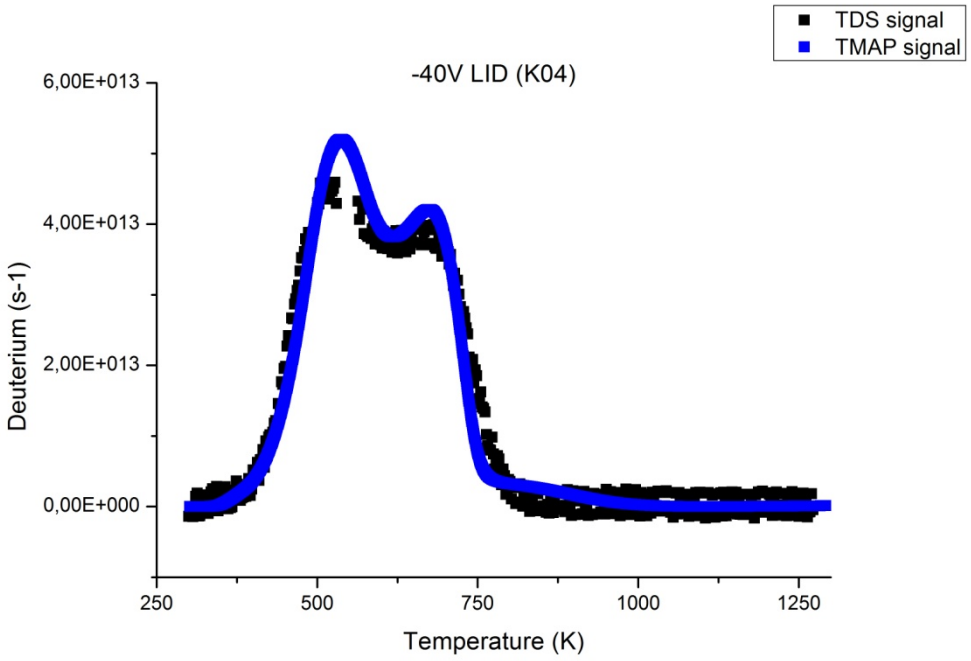

figure 26

TMAP7 fit of the TDS profile of sample K04 (-40V series 3). Information about the deuterium input profile obtained by making this fit are displayed in table 5.

table 3

The results of the TDS simulations of sample R01.1 and R02.2. The trapping energy of trap 1 is $E_{t1} = 1.1\ eV$ and the trapping energy of trap 2 is $E_{t2} = 1.7\ eV$.

Sample	Trap density trap 1	Trap depth trap 1 (m)	Trap density trap 2	Trap depth trap 2 (m)
R01.1	2,00E-05	5,00E-05	0,00E+00	0,00E+00
R02.1	2,00E-05	4,00E-05	0,00E+00	0,00E+00

table 4

The results of the TDS simulations of the bias scan. The trapping energy of trap 1 is $E_{t1} = 1.1\ eV$ and the trapping energy of trap 2 is $E_{t2} = 1.7\ eV$.

Sample	Trap density trap 1	Trap depth trap 1 (m)	Trap density trap 2	Trap depth trap 2 (m)
Floating (R12)	2,00E-05	5,00E-06	1,20E-03	2,00E-07
-10V (R06)	2,00E-05	1,25E-05	0,00E+00	0,00E+00
-20V LID (R08)	2,00E-05	8,00E-06	2,00E-03	2,00E-07
-30V LID (R09)	2,00E-05	4,00E-05	2,00E-03	1,50E-07
-40V LID (R07)	2,00E-05	3,00E-05	2,50E-03	2,00E-07

table 5

The results of the TDS simulations of the undamaged targets of series 3. The trapping energy of trap 1 is $E_{t1} = 1.1\ eV$ and the trapping energy of trap 2 is $E_{t2} = 1.7\ eV$.

Sample	Trap concentration trap 1	Trap depth trap 1 (m)	Trap concentration trap 2	Trap depth trap 2 (m)
-40V LID (K01)	2,00E-05	3,00E-05	2,00E-03	1,50E-07
-40V (K02)	2,00E-05	1,50E-05	2,00E-03	1,00E-07
-40V (K03)	2,00E-05	4,00E-05	2,00E-03	1,50E-07
-40V LID (K04)	2,00E-05	4,00E-05	2,00E-03	1,50E-07

table 6

The results of the TDS simulations of the damaged samples FF12 and FF15. The trap energies are given by $E_{t1} = 1.1\ eV$ $E_{t2} = 1.3\ eV$ $E_{t3} = 2.05\ eV$.

Sample	Trap density trap 1	Trap depth trap 1 (m)	Fill factor trap 1	Trap density trap 2	Trap depth trap 2 (m)	Fill factor trap 2	Trap density trap 3	Trap depth trap 3 (m)	Fill factor trap 3
-40V LID (FF12)	5,00E-03	8,00E-07	0,3	1,50E-03	8,00E-07	0,2	7,00E-03	8,00E-07	1,0
-40V (FF15)	5,00E-03	8,00E-07	0,2	1,50E-03	8,00E-07	0.15	7,00E-03	8,00E-07	1,0

6. Discussion

6. 1 Plasma exposures

Plasma exposures are done with Pilot-PSI. To test the applicability of LID-QMS deuterium implanted targets are analyzed. In a perfect case scenario one would have identical implanted targets available. These are not available however, so deuterium is implanted by exposing samples to deuterium plasmas. Implantation with MAGNUM-PSI and analysis with LID-QMS directly after exposure is investigated. Exposure is too time consuming due to cooling limitations of MAGNUM-PSI to reach sufficient implantation during available experimental times. Another limitation of using MAGNUM-PSI for exposures lies in the fact that the deuterium background signal is too high directly after exposures to measure with the QMS. The minimum pumping down time is two days making it impossible to use LID-QMS as an instantaneous diagnostic. Therefore Pilot-PSI is used to expose samples to deuterium plasma. To compare different samples, samples are exposed to similar plasma fluences. Uncertainties arise in LID-QMS measurements when irregularities during plasma exposure occur. Irregularities can possibly be caused by a decaying magnetic field (during longer shots) or a degrading plasma source. Irregularities can lead to inhomogeneous surface modifications. Inhomogeneous surface modifications are indicated to seriously influence the consistency of LID-QMS measurements.

6.2 Desorption area determination

For the quantification of LID-QMS it is extremely important to properly determine the desorption area. To be able to make the comparison with TDS the signals are expressed in deuterium per square meter. The desorption area is determined in three steps:

1. Determination laser irradiated area
2. Determination temperature dependent spot size on the target
3. Correction for desorption dependency on surface temperature

In previous LID-QMS experiments by Charlie Spork [30] no surface temperature dependency of deuterium desorption is taken into account. Therefore a correction for the theoretical desorption dependency on surface temperature calculated with TMAP7 simulations is included in the desorption area determination in this work. Possible influences of trapping depth on desorption are included in the error analysis of the desorption area.
Correcting the temperature dependent spot size for the desorption dependency on surface temperature gives the radius of the desorption area: $r = 1{,}3\ mm$. Error analysis results in an error of $10\ \%$. The radius is proven to be constant over the different measurement series. Assumptions in this desorption area determination are in the TMAP7 simulations of the desorption dependency on surface temperature. Values for the trap energy and the trap density are included in the simulations. Uncertainties in these assumptions are minimized by checking the values with literature [8][24][25][26][27] and by using the same values for all simulations in this work. Assumptions used are validated for samples and exposure conditions used in this work.

6.3 LID-QMS measurements

The error in the QMS signal is determined to be 8 % using Poisson statistics [28]. This is the statistical standard deviation using Poisson statistics for the number of counts. The error in the QMS signal and the error in the desorption area both contribute to the error in the LID-QMS signal. The error is calculated using standard error propagation [19].

LID-QMS was performed before at DIFFER by Bas Hensen [12] and Charlie Spork [30]. Bas Hensen measured the amount of deuterium retained for multiple laser shots at one location. The amount of deuterium desorbed in the first shot is in accordance with the results in this work. In the work of Charlie Spork the radial flux profile of the plasma exposures is represented by the LID-QMS measurements. Discrepancies between deuterium desorption by LID-QMS and total deuterium desorption signals were observed, caused by problems in the absolute calibration. In this work the calibration is improved by improving the desorption area determination.

LID-QMS analysis of standard polished tungsten samples shows desorption signals similar to the total deuterium desorption signals (sum of LID-QMS and TDS results), indicating the possibility to use LID-QMS without calibration with TDS. As several assumptions are included in this calibration, the calibration can only be used when analyzing similar samples exposed to similar fluences. In other scenarios calibration against TDS is recommended to check whether the assumptions are valid. Comparing the results to the plasma flux profiles sometimes shows inconsistencies. The hypothesis is stated that inhomogeneous surface modifications could influence desorption signals by LID-QMS. Blisters will be destroyed by laser irradiation leading to the desorption of trapped deuterium. This hypothesis is checked with TDS and by making surface pictures by optical microscopy and SEM. Inconsistencies between LID-QMS profiles and plasma profiles are observed in series 2 and 3, but not in series 1. Series 1 is checked for the hypothesis stated anyway to exclude any random effects.

LID-QMS performed on the damaged target FF12 shows desorption lower than the total deuterium desorption signal. This is hypothesized to be due to the presence of high energy traps in the material. Only one set of damaged targets is analyzed, one with both LID-QMS and TDS and one with only TDS. Therefore only an indication of the influence of high energy traps can be provided.

6.4 TDS measurements

TDS analysis is performed to check total deuterium desorption. In series 1 and 3 samples are exposed in pairs to check whether LID-QMS influences TDS profiles measured. No influence of LID-QMS measurements on TDS profiles is observed. Profiles are similar and no shift in between peaks is observed. No damage resulting in new traps is created because no difference in peak locations in between profiles of samples analyzed with LID-QMS compared to samples not analyzed with LID-QMS is observed. TDS profiles of series 1 only show a low temperature peak while the rest of profiles show both a low and a high temperature peak. The high temperature peak is assumed to be related to blister formation. No high temperature peaks are observed for series 1, while one would expect the profiles to look like the profiles of the samples exposed with similar bias in series 2 and 3. A possible explanation could be malfunction of the bias during the exposures of series 1. The total deuterium retention is also lower than expected compared to the rest of the measurements. The

comparison between the two damaged targets (FF12 and FF15) shows no influence of LID-QMS on the TDS profiles.

To check deuterium retention dependency on bias voltage of the exposures the samples of the bias scan exposed to similar fluences are analyzed with TDS. Due to uncertainties in integrated fluence and differences in between exposures it is hard to draw conclusions from this measurement but a trend of increasing deuterium retention for increasing negative bias voltage is observed.

TDS is a reliable diagnostic to measure total deuterium retention in a target. Due to the slow heating rate a temperature dependent desorption profile is produced, providing possibilities to determine properties of different traps with TMAP7. Since the sample is kept constant at the maximum temperature for ten minutes it can safely be assumed that all deuterium is desorbed. The reliability of TDS measurements and to possibility to produce temperature dependent desorption profiles make TDS the perfect candidate for cross calibration of LID-QMS. The temperature dependent desorption profile can be simulated with TMAP7 to validate assumption made in the desorption area determination.

6.5 Optical microscope and SEM results

Stated as a hypothesis to explain inconsistencies between LID-QMS signals and the plasma flux profile are inhomogeneous surface modifications. This hypothesis is also checked for series 1.

No blister formation at all is observed in series 1. A possible explanation could be a malfunction of the bias during exposures. Inconsistencies between LID-QMS and plasma flux profiles are observed for samples of series 2 and series 3. Blister formation is shown by optical microscopy and SEM. Sample surfaces are scanned with optical microscopy to check for inhomogeneous surface modifications and to check whether this can be linked to inconsistencies between LID-QMS measurements and the plasma profile. On samples with measured inconsistencies inhomogeneous blister formation and impurities are shown, while no inhomogeneous blister formation is found on samples with LID-QMS profiles representing the plasma flux profile. This supports the hypothesis stated. Inhomogeneous surface modifications indicate irregularities during plasma exposures but these cannot be specified. Inhomogeneous blister formation can lead to discrepancies between LID-QMS and total desorption signals when the local blister density in the desorption area differs from the average blister density. This results in an under- or overestimation of the local deuterium desorption compared to the total deuterium desorption signal. The levels of the LID-QMS signals measured seem to be quantitatively correct. Irregularities are not caused by problems with the LID-QMS calibrations but by irregularities during plasma exposures.

6.6 TDS simulations

TDS simulations are executed to obtain information about the deuterium implantation profile. The main problem of simulating TDS profiles with LID-QMS is the non-uniqueness of results found. To minimize this uncertainty natural trap energies and trap densities are kept constant for all standard tungsten samples. The trap energy of blisters is also kept constant, but the blister density is varied since this is dependent on the blister density on the surface. Since the trap density of natural trap sites is low all traps are assumed to be completely filled ($fill\ factor = 1$). Values kept constant are

compared to values available in literature [8][24][25][26][27] to further decrease the uncertainty. Although uncertainties are minimized as described it is still dangerous to draw solid conclusion based on TMAP7 simulations. The non-uniqueness of results and the assumptions made always have to be kept in mind.

Simulations of the TDS profiles of standard samples seem to validate the assumptions on trap energy, density and trapping depth made in the desorption area determination. Blister presence is shown by the TDS simulations for the standard tungsten samples used. TMAP7 simulations of the TDS profiles of the damaged targets indicate that deuterium desorption is limited by deuterium trapped in high energy traps: for both damaged targets the high energy traps are completely filled indicating that deuterium desorption from these traps by LID-QMS is impossible.

7. Conclusion

In this work the working principles and the applicability of laser-induced desorption quadruple mass spectrometry (LID-QMS) are reviewed. Several experimental series are conducted with targets exposed to deuterium plasma in Pilot-PSI. The first goal of these experiments was to understand processes involved in deuterium desorption by LID-QMS and to determine the possibilities of LID-QMS. LID-QMS results are compared to total deuterium desorption signals (the sum of LID-QMS and TDS results) to check whether interpretation of LID-QMS is possible without calibration with TDS and to check the influence of LID-QMS on TDS profiles. The deuterium retention dependency of bias is also looked into. Theoretical modeling using TMAP7 is conducted to get a better insight in the phenomena observed.

The desorption area is the most important quantification of LID-QMS. To be able to perform comparisons between LID-QMS and total deuterium desorption, LID-QMS signals are expressed in deuterium per square meter. Desorption is $< 100\ \%$ for lower surface temperatures. Not all the deuterium is desorbed from the laser heated area, since part of this area does not reach sufficient surface temperatures. Desorption percentage dependency on surface temperature is simulated with TMAP7. The desorption area is determined by correcting the heated area for desorption dependency on surface temperature. Part of the heated area is excluded from the desorption area. This part excluded corrects for the part where 100% desorption is theoretically not possible. A temperature limit is now determined where this correction theoretically results in $100\ \%$ desorption. The error margin due to possible differences in implantation depth is set to be $10\ \%$. The surface area corresponding to this temperature is set to be the desorption area. The radius of the desorption area is shown to be $r = 1{,}3\ mm$.

Assumptions about the trap energy and trap density in tungsten are necessary for the desorption area determination. Uncertainties arising from assumption on the trapping depth are included in the error analysis. Due to these assumptions absolute calibration of LID-QMS can only be concluded to be working for standard tungsten samples without created damage with deuterium implantation depths according to fluences up to $3 \cdot 10^{26}\ m^{-2}$. Inconsistencies observed are due to irregularities in blister formation probably arising from irregularities during plasma exposures. This statement is supported by optical microscopy pictures.

LID-QMS results are also conducted on damaged targets with known trap energies, depths and densities. LID-QMS results are located significantly below the total deuterium desorption signals. Comparing TDS results and their fits with TMAP7 of the sample analyzed with both LID-QMS and TDS and the sample only analyzed with TDS shows that for both samples the high energy traps are completely filled. This supports the hypothesis stated that deuterium trapped in high energy traps cannot be desorbed with LID-QMS.

For samples exposed in other machines or to higher fluences and accompanying higher deuterium implantation depths extra TMAP7 LID-QMS simulations have to be conducted for the determination of the desorption area. For LID-QMS simulations to be executed TDS measurements have to be conducted and simulated to obtain knowledge about the implantation profile. In this case absolute calibrations is therefore not possible.

7.1 Recommendations for further research

The applicability of LID-QMS is linked to the fluence achieved during exposures. To increase the possible uses for LID-QMS the desorption area can be determined for targets exposed to higher fluences. To do this a measurement series comparable to series 3 has to be conducted for significantly higher fluences. Calibration with TDS and simulations with TMAP7 have to executed to determine the desorption area. If the deuterium implantation depth can be directly linked to fluence, the applicability of LID-QMS could be linked to fluence. If desorption area determinations like conducted in this work are to be executed for the range of fluences and according implantation depths achievable with Pilot-PSI LID-QMS can in theory be used to determine the local deuterium inventory. Irregularities might still arise, but these are indicated to be the effect of plasma exposures and not the effect of irregularities in LID-QMS.

Laser parameters and the maximum surface temperature are kept approximately constant in this work. Simulations can be conducted with TMAP7 to check the influence of changing the surface temperature on implantation depth dependence of desorption. The influence of increasing the pulse duration can also be simulated to see if this could theoretically increase deuterium desorption. If modeling shows possible improvements, actual experiments can be conducted to confirm these improvements.

Development of the ion current measured with the QMS after the laser shot is executed are not completely understood. Possible explanations are provided: spreading of deuterium over the vacuum vessel (short timescale) or sticking of deuterium to the vacuum vessel. By replacing the LID-QMS setup to a smaller vacuum vessel more knowledge about the behavior of the ion current can be acquired.

Appendices

A1. Plasma fluence

The plasma flux can be calculated using two methods. The first method uses the measured ion-saturation current to calculate the flux Γ. The ion-saturation current is measured during the exposure and can be used to determine the flux:

$$\Gamma_{av}(\mathrm{r}) = \frac{I_{sat}}{e\pi r^2} \quad (7)$$

where *e* is the elementary charge and *r* is the radius of your exposed surface. The ion saturation current is the combined current on the target and the clamping ring. An estimation has to be made to decide what part of the ion saturation current is said to arrive on the target. This flux calculation is used in the beginning of the experiments for comparison with the second flux calculation method.

The second method uses the radial Thomson Scattering data to calculate the flux Γ on the target. The local flux at distance r from the centre can be calculated using [29]:

$$\Gamma(\mathrm{r}) = \frac{1}{2} n_e(r) \sqrt{\frac{k_b(T_i(r) + \gamma T_e(r))}{m_i}} = \frac{1}{2} n_e(r) \sqrt{\frac{k_b(\gamma + 1) T_e(r)}{m_i}} \quad (8)$$

In this formula it is assumed that $T_e = T_i$. The electron density n_e and electron temperature T_e are obtained from Thomson Scattering data. The specific heat ratio is assumed to be $\gamma = 5/3$ and m_i and k_b are given by the deuterium ion mass and the Boltzmann constant respectively. This formula can be used to calculate the flux at each radial location of your sample. The flux averaged over the surface can be obtained by integrating the radial flux over the exposed surface of you sample:

$$\Gamma_{\mathrm{av}} = \frac{1}{\pi r^2} \int_0^r \Gamma(\mathrm{r}) 2\pi \mathrm{r} \mathrm{dr} \quad (9)$$

where r is the radius of the exposed sample. Instead of the average flux the maximum flux is used in this work to simplify comparisons during exposures.

The fluence F can now calculated by multiplying the calculated flux by the exposure time *t*:

$$F = \Gamma \cdot \mathrm{t} \quad (10)$$

A2. TDS profiles

The complete TDS profiles of the bias scan are plotted in figure 27. The integrated results are discussed in section 5. Results.

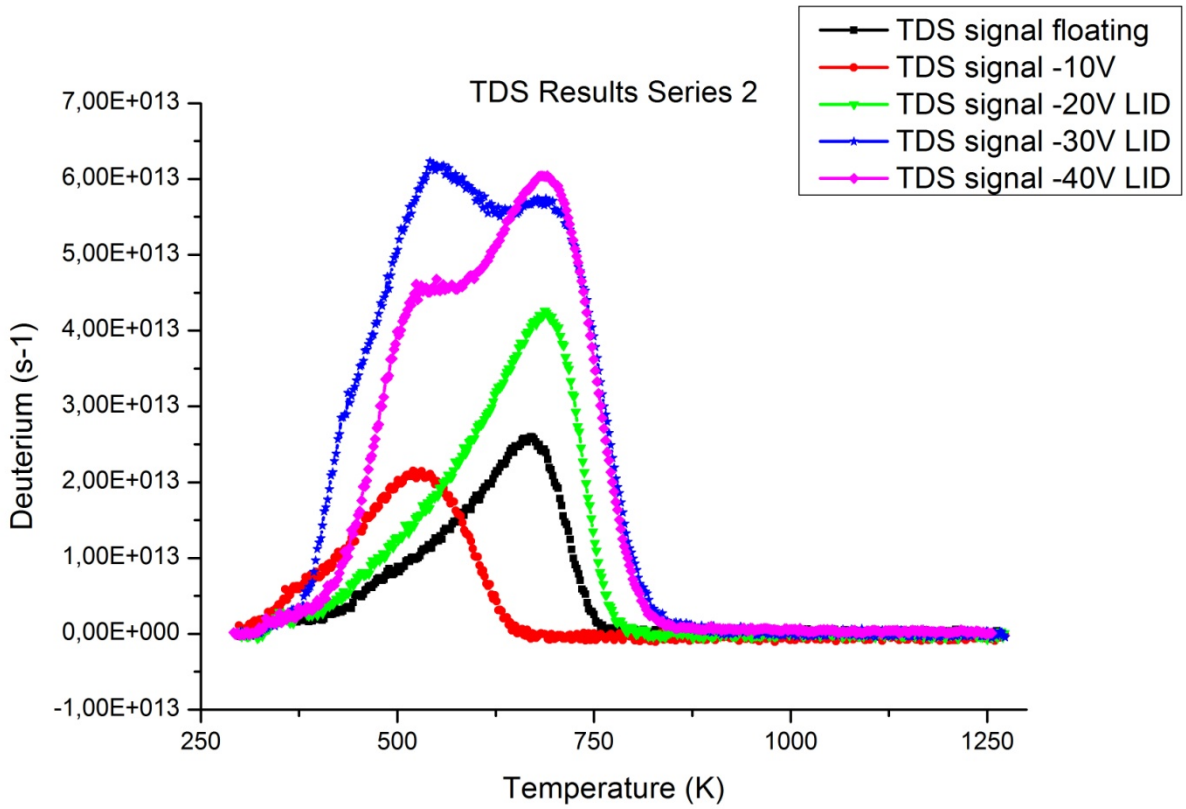

figure 27

TDS profiles of the bias scan. A trend of increasing deuterium retention for increasing negative bias voltage is observed. Saturation at -30V bias is observed within the error margins of the measurements.

A3. Optical microscope and SEM pictures

In this section the optical microscope pictures described in section 5.4 are displayed. From the picture inhomogeneous blister formation is observed at location exposed to similar plasma fluxes and fluences. It was hypothesized that inconsistencies in measured LID-QMS signals could be the result of this inhomogeneous blister formation.

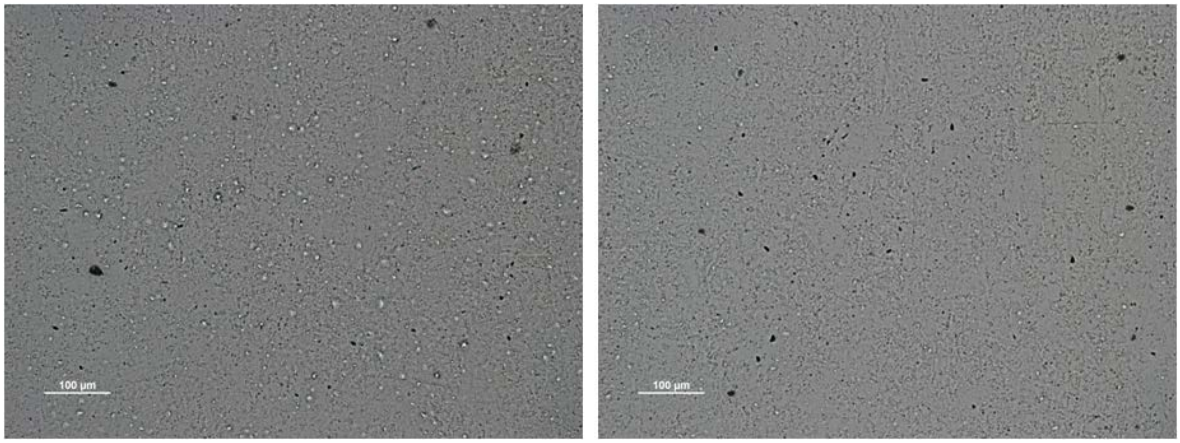

figure 28

Surface pictures sample R08. Inhomogeneous blister formation is observed: blister formation in the left picture is clearly present while hardly any blister formation is observed in the right picture.

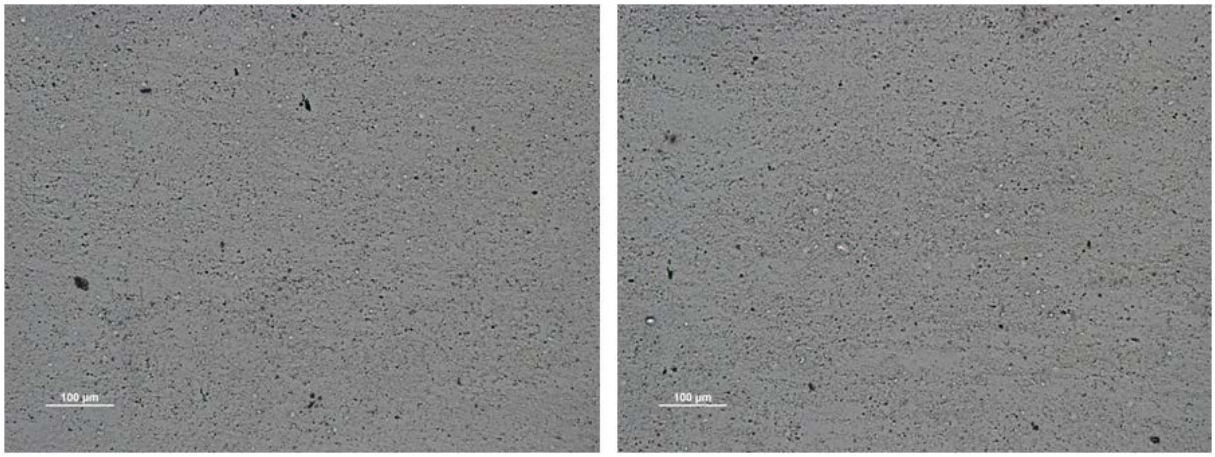

figure 29

Surface pictures sample K04. Inhomogeneous blister formation is observed: blister formation in the right picture is clearly present while hardly any blister formation is observed in the left picture.

figure 30

Surface pictures sample R09. No inhomogeneous surface modifications are observed.

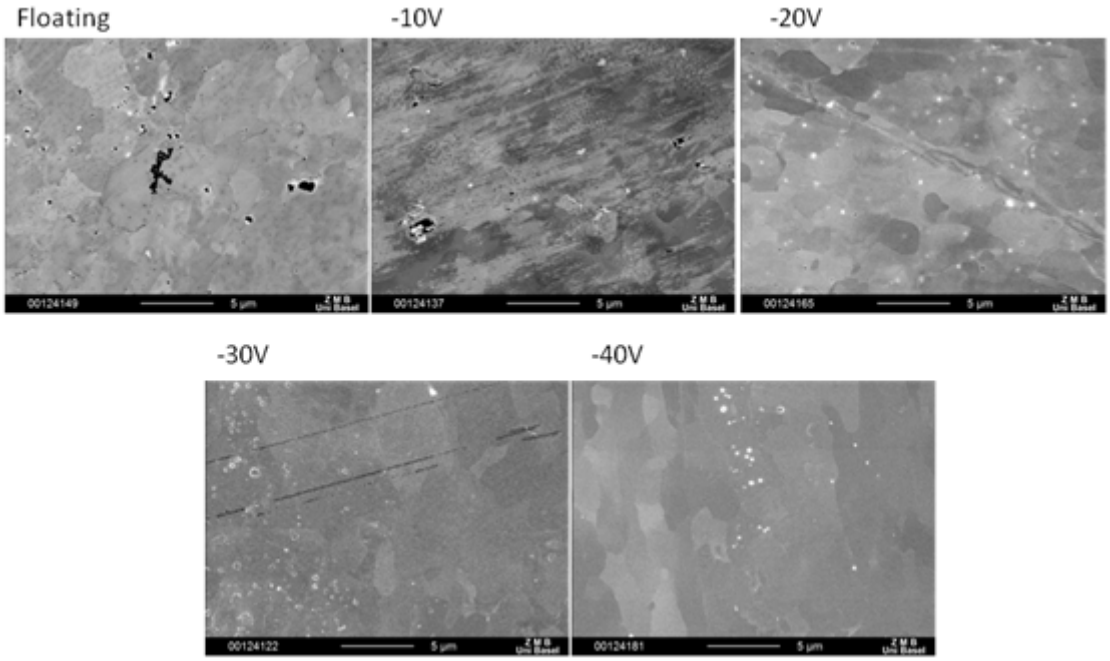

figure 31

SEM images of the samples of the performed bias scan: magnification = 5000x.

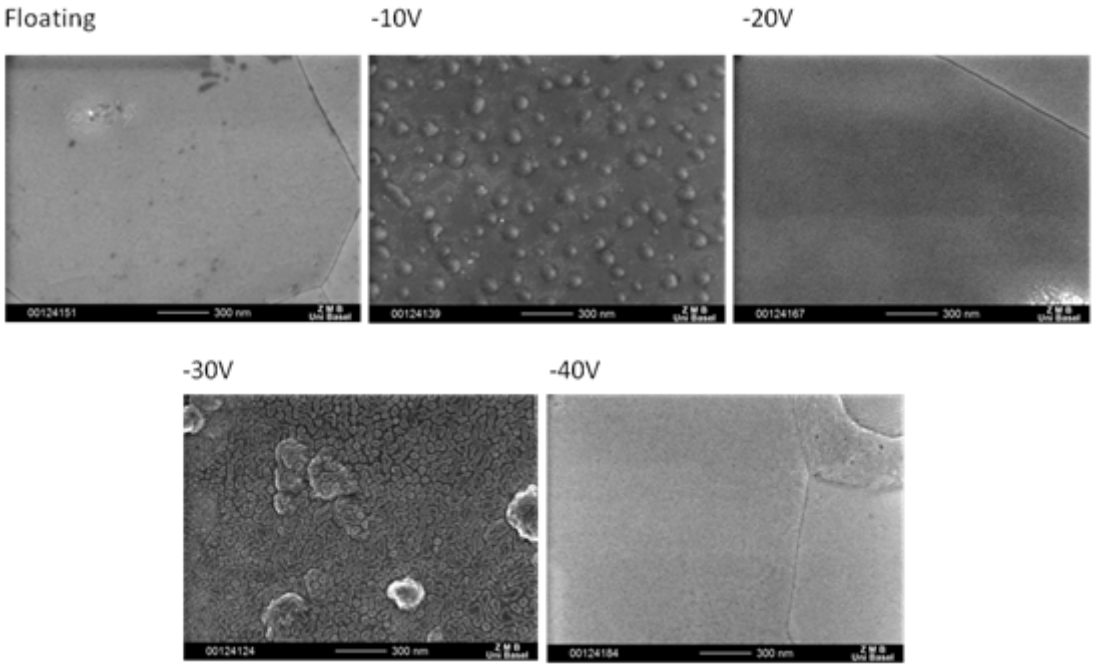

figure 32

SEM images of the samples of the performed bias scan: magnification = 60000x.

A4. TMAP7 simulation TDS profiles

In this section the plots of the TMAP7 simulations of the TDS profiles are displayed. The simulations are displayed per measurement series. The resulting implantation profiles are discussed in the simulation results

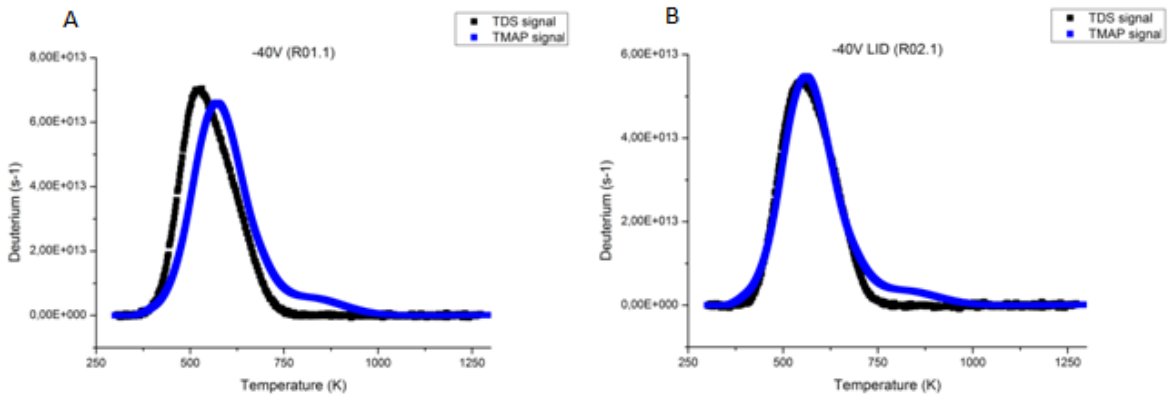

figure 33

TMAP7 simulations of the TDS profiles of sample R01.1 (A) and R02.1 (B). Sample R01.1 is only analyzed with TDS while sample R02.1 is also analyzed with LID-QMS

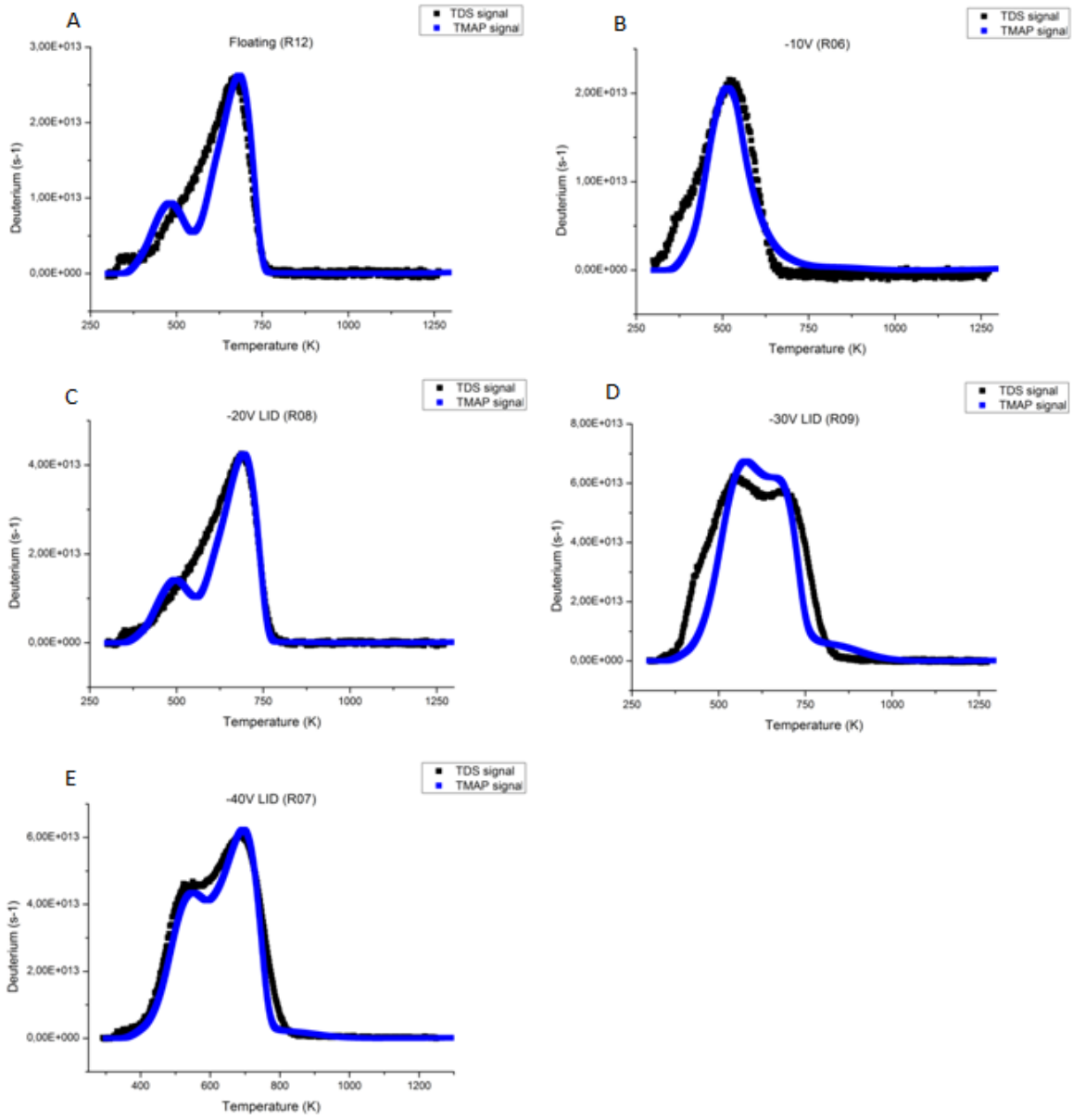

figure 34

TMAP7 simulations of the TDS profiles of the floating, -10V, -20V, -30V and -40V biased samples (A-E). The -20V, -30V and -40V are analyzed with both LID-QMS and TDS, while the rest is only analyzed with TDS.

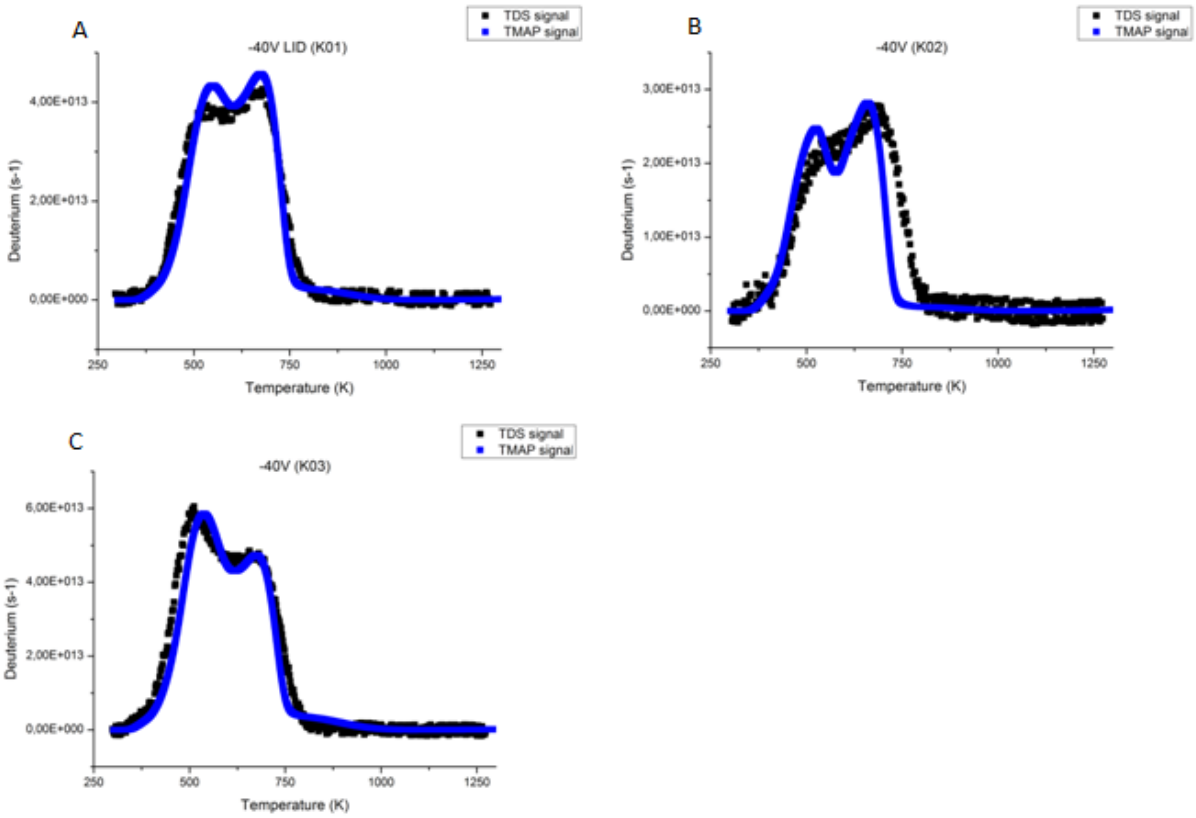

figure 35

TMAP7 simulations of the TDS profiles of sample K01 (A), K02 (B) and K03 (C). K03 is analyzed with both LID-QMS and TDS, while the rest is only analyzed with TDS.

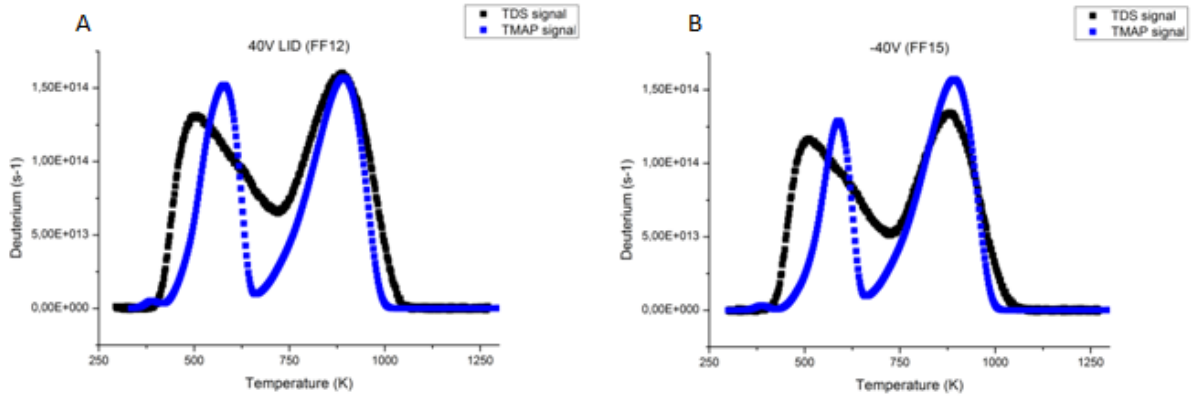

figure 36

TMAP7 simulations of the TDS profiles of sample FF12 (A) and FF15 (B). FF12 is analyzed with both LID-QMS and TDS, while FF15 is only analyzed with TDS.

A5. TMAP input files

In this section two examples of input files are given: an example of a TDS measurement simulation and an example of a LID measurement simulation. The main difference between these two simulations is the heating rate of the samples. Similar implantation profiles are used.

In both models a tungsten sample of 1 mm thickness is used. The sample is divided into 66 nodes as illustrated in figure 37 [30]. Node is the definition given in the TMAP7 manual [22]. To prevent confusion about this term, the term segment will be used in this work. At each segment and for each time step relevant physical quantities are calculated. In these simulations the relevant physical quantities are the particle flux leaving the surface, the temperature and the trapped and mobile deuterium concentrations.

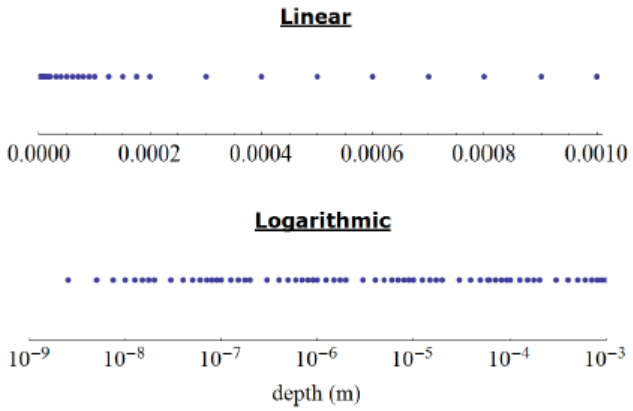

figure 37

Different segments for which the relevant physical quantities are determined. For each segment the temperature and the trapped and mobile deuterium concentrations are displayed in the output file. The particle flux leaving the target is also executed.

To perform the simulations several boundary conditions have to be implemented in the model. The input parameters essential to define are divided in three main categories: the enclosure input, the thermal input and the diffusion input. In TDS simulations the trap information, defined in the diffusion input, is varied to get an optimal fit to the data. In LID-QMS simulations the main goal is to determine the percentage of hydrogen desorbed. LID-QMS measurements on samples with retention profiles like determined with TDS simulations are simulated.

A5.1 Enclosure input

With TDS simulations the enclosure is defined as the vacuum vessel of the TDS setup, with LID-QMS simulations the enclosure is defined to be the TEAC of MAGNUM-PSI. The starting temperature of the enclosure of the sample is set to be $300K$. The enclosure is assumed to be filled with gas consisting of D2 molecules at a partial pressure of $1 \cdot 10^{-6} Pa$ (vacuum). The temperature and pressure can be changed.

A5.2 Thermal input

In the thermal input the segments, as described in figure 37, and the starting temperature of the sample ($300K$) are defined. The heating rate of the front- and the back-side of the surface are defined in the thermal input as well. For TDS simulations the front- and back-side temperatures are assumed to be similar, for LID simulation the back-side temperature of the sample is assumed to remain constant at $300K$.

A5.3 Diffusion input

The implanted deuterium profile is defined in the diffusion input. The parameters to define are the trap-concentration, trap-depth, traps filled and the fill factor of the traps filled. Up to three traps can be inserted. By adjusting this profile a fit of TDS measurements can be produced.

In section A5.4 TDS desorption simulation and section A5.5 LID desorption simulation the complete input files used for TDS and LID-QMS simulations are displayed.

A5.4 TDS desorption simulation

```
$ Details can be found in the TMAP7 manual. Dollar signs in front of text indicates comment.
$ ---------------------------
title input                         $ Title input can be used to give details about the simulation.
$ ---------------------------
polyX tungsten, no implantation
no cooldown sample in 2s to 300K
TDS at 1 K/s to 1300K
Traps: 1.2eV(1mm)/ 1.4eV(1um)/ 1.85eV(0um)
end of title input
$ ---------------------------
main input
$ ---------------------------
dspcnme=d,end                       $ diffusive species
sspcnme=d2,end                      $ surface species
espcnme=d2g,end                     $ enclosure species
segnds=66,end                       $ segments with #nodes (this case 1 segment with 66 nodes)
nbrencl=1,end                       $ 1 test chamber
end of main input
$ ---------------------------
enclosure input
$ ---------------------------
start bdry,1,end                    $ boundary condition for enclosure 1
$ Enclosure 1 is the plasma chamber with pressure assumed negligible
etemp=300.0,end                     $ temperature in K
esppres=d2g,const,1.0e-6,end        $ pressure in Pa
end of enclosure input
$ ---------------------------
thermal input
$ ---------------------------
start thermseg,end
delx=0.0,8*2.5e-9,8*1e-8,4*2.5e-8,8*1e-7,4*2.5e-7,8*1e-6
4*2.5e-6,8*1e-5,4*2.5e-5,8*1e-4,0.0,end
$ nodal separation in m, first and the last node must be equal to unity, number must equal segnds
tempd=const,300.0,end               $ initial temperature distribution in K
tcon=equ,1,end                      $ thermal conductivity of W in W/m K(equation 1)
rhocp=equ,2,end                     $ thermal capacity of W in J/m3K
```

```
hsrc=const,0.0,srcpf,const,0.0,end
$ neglect internal heat generation rate/ spacial distr& source peaking factor
htrbcl=stemp,tabl,1,end
$ temperature in K on the plasma-side surface, boundary conditions for heat transfer calculations
htrbcr=stemp,tabl,1,end
 $ temperature in K on the back-side surface
end of thermal input
$ --------------------------
diffusion input
$ --------------------------
start diffseg,end
nbrden=6.28e28,end                    $ lattice number density of tungsten in atoms/m3 (19.3*1e3/(183.84*1.67e-27))
concd=d,const,0.0,end                 $ initial mobile D concentration in atoms/m3 (zero is accurate for long time delay
between exposure and desorption)
ssconc=d2,0.0,0.0,end                 $ initial surface species concentration atoms/m3
trapping=ttyp,1,tconc,0.0,64*2.0e-5,0.0        $ natural traps - whole depth range
          tspc,d,alphr,equ,4,alpht,equ,3
          ctrap,0.0,64*0.0,0.0
       ttyp,2,tconc,0.0,64*2.0e-5,0.0           $ ion damage - 1um depth
          tspc,d,alphr,equ,5,alpht,equ,3
          ctrap,0.0,45*1.0,19*0.0,0.0
       ttyp,3,tconc,0.0,20*0.0025,44*0.0,0.0    $ ion damage - 1um depth
          tspc,d,alphr,equ,6,alpht,equ,3
          ctrap,0.0,20*1.0,44*0.0,0.0,end
qstrdr=d,const,0.,end
$ Q*/R for Soret effect unknown - not relevant since sample has homogeneous temperature (diffusion coefficient for
thermal diffusion)
dcoef=d,equ,7,d2,equ,8,end                    $ diffusion coefficient (m2/s)
$srcsd=d,tabl,2,srcpf,0.0,0.5,63*0.0,0.0,end
$ volumetric production or annihilation (srcsd), peak factor (srcpf) depth distribution of diffusing species
srcsd=d,const,0.0,srcpf,const,0.0,end    $ in case of no implantation
difbcl=surfdep,encl,1
  spc,d,nu,8.4e12,ec,-0.4,es,1.04
    comb,d,prob,1.0
  spc,d2,nu,8.4e12,ec,-0.1
    exch,d2g,amu,4.0,ex,0.05
    diss,d,d,eb,0.05
    form,d,d,prob,1.0,end
difbcr=surfdep,encl,1
  spc,d,nu,8.4e12,ec,-0.4,es,1.04
    comb,d,prob,1.0
  spc,d2,nu,8.4e12,ec,-0.1
    exch,d2g,amu,4.0,ex,0.05
    diss,d,d,eb,0.05
    form,d,d,prob,1.0,end
$difbcl=ratedep,encl,1,spc,d,exch,d2g,ksubd,equ,9,d,ksubr,equ,10,end  $ in case of ratedependent surface reactions
$difbcr=ratedep,encl,1,spc,d,exch,d2g,ksubd,equ,9,d,ksubr,equ,10,end  $ in case of ratedependent surface reactions
$ in case of ratedependent surface reactions
$ --> remove $sspcnme $ssconc
$ --> change $dcoef=d,equ,7
$ --> add
$    $ (9) Dissociation coefficient (ksubd)
$      y=1.09e34*exp(-3.24/8.618e-5/temp),end
$    $ (10) Recombination coefficient (ksubr); Ogorodnikova theory Ec = 0.2 eV
$      y=3.2e-15*exp(-1.16/8.618e-5/temp),end
$    $
surfa=0.0002,end
end of diffusion input
$ --------------------------
equation input
$ --------------------------
$ (1) Thermal conductivity of tungsten (W/m-K), fitted from ANSIS data
    y=-5.686e-8*temp**3+2.0428e-4*temp**2-0.26620*temp+236.22,end
```

```
$ (2) Rho Cp for tungsten (J/m3K), fitted from ANSIS data
    y=7.0046e-5*temp**3-1.6608e-1*temp**2-5.0940e2*temp+2.3937e6,end
$ (3) Alpht for d in tungsten (1/s)
    y=2.9e12*exp(-0.39/8.625e -5/temp),end
$ (4) Alphr for trap 1 in tungsten (1/s)
    y=8.4e12*exp(-0.9/8.625e-5/temp),end
$ (5) Alphr for trap 2 in tungsten (1/s)
    y=8.4e12*exp(-1.1/8.625e-5/temp),end
$ (6) Alphr for trap 3 in tungsten (1/s)
    y=8.4e12*exp(-1.7/8.625e-5/temp),end
$ (7) Diffusivity for d in tungsten (m2/s)
    y=2.9e-7*exp(-0.39/8.625e-5/temp),end
$ (8) Surface diffusivity for d2 at tungsten surface (m2/s)
    y=2.0e-7*exp(-0.1/8.625e-5/temp),end
end of equation input
$ ---------------------------
table input
$ ---------------------------
$ (1) Surface temperature sample (K)
0.,300.
1000.,1300.,end
$ (2) Implantation flux (atom/m2/s)
0.,0.0
1000.,0.0,end
end of table input
$ ---------------------------
control input
$ ---------------------------
time=0.,end                     $ Initializing time at 0.0
tstep=.5,end                    $ Size of each time step
timend=1000.,end                $ Defining the finishing point
nprint=1,end                    $ The number of tstep cycles skipped between output listings of the results (.out)
itermx=100000,end               $ Number of iterations before the program stops;   Poon = 10000, default = 1000
delcmx=1.e-6,end
$ Convergence limit;                                Poon = 1.0e-6, default = 1.0e-7
bump=1.e-4,end
$ Fractional change in dependent variable value used in the process of Newton-Raphson convergence Poon=1.0e-4 default
1.0e-2
bound=3.0,end
$ Maximum iterative variable increase factor;    Poon = 5.0, default = 2.0
omega=0.9,end
$ Damping factor to improve convergence;            Poon = 0.9, default = 1.3
damp=0.9,end
$ Damping factor to improve convergence;            Poon = 0.9, default = 0.7
end of control input
$ ---------------------------
plot input
$ ---------------------------
nplot=1,end                     $ The number of tstep cycles skipped between output listings of the results (.plt)
plotseg=1,end                   $ Which segments are to be included in plot
plotencl=1,end                  $ Which enclosures should be plotted
dname=d,end                     $ Which diffusion species are to be plotted
sname=end                       $ Which surface species are to be plotted
ename=end                       $ Which enclosure species are to be plotted
dplot=moblinv,sflux,trapinv,end $ Which parameters of diffusion species are to be plotted
eplot=end                       $ Which parameters of enclosure species are to be plotted
end of plot input
$ ---------------------------
end of data
```

A5.5 LID desorption simulation

```
$ Details can be found in the TMAP7 manual. Dollar signs in front of text indicates comment.
$ -------------------------
title input                                   $ Title input can be used to give details about the simulation.
$ -------------------------
polyX tungsten, no implantation
no cooldown sample in 2s to 300K
TDS at 1 K/s to 1300K
Traps: 1.2eV(1mm)/ 1.4eV(1um)/ 1.85eV(0um)
end of title input
$ -------------------------
main input
$ -------------------------
dspcnme=d,end                         $ diffusive species
sspcnme=d2,end                        $ surface species
espcnme=d2g,end                       $ enclosure species
segnds=66,end                         $ segments with #nodes (this case 1 segment with 66 nodes)
nbrencl=1,end                         $ 1 test chamber
end of main input
$ -------------------------
enclosure input
$ -------------------------
start bdry,1,end                      $ boundary condition for enclosure 1
$ Enclosure 1 is the plasma chamber with pressure assumed negligible
etemp=300.0,end                       $ temperature in K
esppres=d2g,const,1.0e-6,end          $ pressure in Pa
end of enclosure input
$ -------------------------
thermal input
$ -------------------------
start thermseg,end
delx=0.0,8*2.5e-9,8*1e-8,4*2.5e-8,8*1e-7,4*2.5e-7,8*1e-6
4*2.5e-6,8*1e-5,4*2.5e-5,8*1e-4,0.0,end
$ nodal separation in m, first and the last node must be equal to unity, number must equal segnds
tempd=const,300.0,end                         $ initial temperature distribution in K
tcon=equ,1,end                        $ thermal conductivity of W in W/m K(equation 1)
rhocp=equ,2,end                       $ thermal capacity of W in J/m3K
hsrc=const,0.0,srcpf,const,0.0,end
$ neglect internal heat generation rate/ spacial distr& source peaking factor
htrbcl=stemp,tabl,1,end
$ temperature in K on the plasma-side surface, boundary conditions for heat transfer calculations
htrbcr=stemp,tabl,1,end
$ temperature in K on the back-side surface
end of thermal input
$ -------------------------
diffusion input
$ -------------------------
start diffseg,end
nbrden=6.28e28,end                    $ lattice number density of tungsten in atoms/m3 (19.3*1e3/(183.84*1.67e-27))
concd=d,const,0.0,end                 $ initial mobile D concentration in atoms/m3 (zero is accurate for long time delay
between exposure and desorption)
ssconc=d2,0.0,0.0,end                 $ initial surface species concentration atoms/m3
trapping=ttyp,1,tconc,0.0,64*5.0e-5,0.0       $ natural traps - whole depth range
        tspc,d,alphr,equ,4,alpht,equ,3
        ctrap,0.0,44*1.0,20*0.0,0.0
    ttyp,2,tconc,0.0,64*0.0,0.0       $ ion damage - 1um depth
        tspc,d,alphr,equ,5,alpht,equ,3
        ctrap,0.0,64*0.0,0.0
    ttyp,3,tconc,0.0,64*0.0,0.0       $ ion damage - 1um depth
        tspc,d,alphr,equ,6,alpht,equ,3
```

```
          ctrap,0.0,64*0.0,0.0,end
qstrdr=d,const,0.,end                    $ Q*/R for Soret effect unknown - not relevant since sample has homogeneous
temperature (diffusion coefficient for thermal diffusion)
dcoef=d,equ,7,d2,equ,8,end               $ diffusion coefficient (m2/s)
$srcsd=d,tabl,2,srcpf,0.0,0.5,63*0.0,0.0,end    $ volumetric production or annihilation (srcsd), peak factor (srcpf) depth
distribution of diffusing species
srcsd=d,const,0.0,srcpf,const,0.0,end        $ in case of no implantation
difbcl=surfdep,encl,1
  spc,d,nu,8.4e12,ec,-0.4,es,1.04
    comb,d,prob,1.0
  spc,d2,nu,8.4e12,ec,-0.1
    exch,d2g,amu,4.0,ex,0.05
    diss,d,d,eb,0.05
    form,d,d,prob,1.0,end
difbcr=surfdep,encl,1
  spc,d,nu,8.4e12,ec,-0.4,es,1.04
    comb,d,prob,1.0
  spc,d2,nu,8.4e12,ec,-0.1
    exch,d2g,amu,4.0,ex,0.05
    diss,d,d,eb,0.05
    form,d,d,prob,1.0,end
$difbcl=ratedep,encl,1,spc,d,exch,d2g,ksubd,equ,9,d,ksubr,equ,10,end  $ in case of ratedependent surface reactions
$difbcr=ratedep,encl,1,spc,d,exch,d2g,ksubd,equ,9,d,ksubr,equ,10,end  $ in case of ratedependent surface reactions
$ in case of ratedependent surface reactions
$ --> remove $sspcnme $ssconc
$ --> change $dcoef=d,equ,7
$ --> add
$    $ (9) Dissociation coefficient (ksubd)
$      y=1.09e34*exp(-3.24/8.618e-5/temp),end
$    $ (10) Recombination coefficient (ksubr); Ogorodnikova theory Ec = 0.2 eV
$      y=3.2e-15*exp(-1.16/8.618e-5/temp),end
$    $
surfa=0.0002,end
end of diffusion input
$ -------------------------
equation input
$ -------------------------
$ (1) Thermal conductivity of tungsten (W/m-K), fitted from ANSIS data
    y=-5.686e-8*temp**3+2.0428e-4*temp**2-0.26620*temp+236.22,end
$ (2) Rho Cp for tungsten (J/m3K), fitted from ANSIS data
    y=7.0046e-5*temp**3-1.6608e-1*temp**2-5.0940e2*temp+2.3937e6,end
$ (3) Alpht for d in tungsten (1/s)
    y=2.9e12*exp(-0.39/8.625e -5/temp),end
$ (4) Alphr for trap 1 in tungsten (1/s)
    y=8.4e12*exp(-1.1/8.625e-5/temp),end
$ (5) Alphr for trap 2 in tungsten (1/s)
    y=8.4e12*exp(-0.9/8.625e-5/temp),end
$ (6) Alphr for trap 3 in tungsten (1/s)
    y=8.4e12*exp(-1.7/8.625e-5/temp),end
$ (7) Diffusivity for d in tungsten (m2/s)
    y=2.9e-7*exp(-0.39/8.625e-5/temp),end
$ (8) Surface diffusivity for d2 at tungsten surface (m2/s)
    y=2.0e-7*exp(-0.1/8.625e-5/temp),end
end of equation input
$ -------------------------
table input
$ -------------------------
$ (1) Surface temperature sample (K)
0.,300.
0.003,2100.
0.006,300.
0.01,300.,end
$ (2) Implantation flux (atom/m2/s)
```

```
0.,0.0
1000.,0.0,end
end of table input
$ --------------------------
control input
$ --------------------------
time=0.,end                          $ Initializing time at 0.0
tstep=.0001,end                        $ Size of each time step
timend=0.01,end                      $ Defining the finishing point
nprint=1,end                         $ The number of tstep cycles skipped between output listings of the results (.out)
itermx=100000,end                      $ Number of iterations before the program stops;    Poon = 10000, default = 1000
delcmx=1.e-6,end                     $ Convergence limit;                    Poon = 1.0e-6, default = 1.0e-7
bump=1.e-4,end                       $ Fractional change in dependent variable value used in the process of Newton-
Raphson convergence Poon=1.0e-4 default 1.0e-2
bound=3.0,end                        $ Maximum iterative variable increase factor;      Poon = 5.0, default = 2.0
omega=0.9,end                        $ Damping factor to improve convergence;          Poon = 0.9, default = 1.3
damp=0.9,end                         $ Damping factor to improve convergence;          Poon = 0.9, default = 0.7
end of control input
$ --------------------------
plot input
$ --------------------------
nplot=1,end                          $ The number of tstep cycles skipped between output listings of the results (.plt)
plotseg=1,end                        $ Which segments are to be included in plot
plotencl=1,end                       $ Which enclosures should be plotted
dname=d,end                          $ Which diffusion species are to be plotted
sname=end                            $ Which surface species are to be plotted
ename=end                            $ Which enclosure species are to be plotted
dplot=moblinv,sflux,trapinv,end              $ Which parameters of diffusion species are to be plotted
eplot=end                           $ Which parameters of enclosure species are to be plotted
end of plot input
$ --------------------------
end of data
```

References

[1] Bong Geun Hong et al, *Basic concepts of DEMO and a design of a helium cooled molten lithium blanket for testing in ITER,* Fusion Engineering and Design 87 (2007) 2399-2405
[2] H.J. de Blank, *PLASMA PHYSICS Lecture Notes,* FOM-Institute for Plasma Physics Rijnhuizen (2011)
[3] J. Roth et al, *Recent alanysis of key plasma wall interations issues for ITER,* Journal of Nuclear Matters 390-391 (2009) 1-9
[4]http://www.iter.org
[5] Rion A. Causey, *Hydrogen isotope retention and recycling in fusion reactor plasma-facing components,* Journal of Nuclear Materials 300 (2002) 91-117
[6] D. Nishijina et al, *Supression of blister formation and deuterium retention on tungsten surface due to mechanical polishing and helium pre-exposure,* Nucl. Fusion 45 (2005) 669-674
[7] K. Tokunaga et al, *Blister formation and deuterium retention on tungsten exposed to low energy and high flux deuterium plasma,* Journal of Nuclear Materials 337-339 (2005) 887-891
[8] M.H.J. 't Hoen et al, *Reduced deuterium retention in self-damaged tungsten exposed to high-flux plasmas at high surface temperatures,* Nuclear Fusion 53 (2013) 043003
[9] R. Causey et al, *Tritium retention in tungsten exposed to intense fluxes of 100 eV tritons,* Journal of Nuclear Materials 266-269 (1999) 467-471
[10] A.A. Haasz et at, *Deuterium retention in tungsten for fusion use,* Journal of Nuclear Materials 258-263 (1998) 889-895
[11] Edward D. Palik, *Handbook of Optical Constants of Solids II,* Academic Press, 1991
[12] Bas Hensen, *Effect of transient heat loads on plasma-exposed tungsten surfaces,* FOM Institute Differ, 2012
[13] Robert W. Serth, *Process Heat Transfer, Principles and Applications,* Academic Press, 2007
[14] H.S. Carslaw and J.C. Jaeger, *Conduction of Heat in Solids,* Oxford University Press, 1989
[15] Erik Lassner and Wolf-Dieter Schubert, *Tungsten: Properties, Chemistry, Technology of the Element, Alloys, and Chemical Compounds,* Kluwer Academic, 1999
[16] M. Zoblinski et al, *Laser induced desorption as tritium retention diagnostic method in ITER,* Fusion Engineering and Design 86 (2011) 1332-1335
[17] H.J. van der Meiden et al, *High sensitivity imaging Thomson scattering for low temperature plasma,* Review of Scientific Instruments 79 (2008) 013505
[18]http://instructor.physics.lsa.umich.edu/adv-labs/Mass_Spectrometer/MassSpecQMS.pdf
[19] John R. Taylor, *An Introduction to Error Analysis: The Study of Uncertainties in Physical Measurements,* University Science Books, 1997
[20] *IDL Tutorial: Programming in IDL.* ITT Visual Information Solutions (2009)
[21] P.A. Redhead, *Thermal Desorption of Gasses,* Radia and Electrical Engineering Division (1962)
[22] G.R. Lonhurst, *TMAP7 User Manual,* Idaho National University INEEL/EXT-04-01657, 2008
[23] M.H.J. 'Hoen, *Saturation of deuterium retention in self-damaged tungsten exposed to high flux plasmas,* Nucl. Fusion 52 (2012) 023008
[24] B. Schweer, *In situ diagnostic for monitoring of deuterium and tritium in re-deposited carbon layers by laser induced desorption,* Journal of Nuclear Materials 363-365 (2007) 1375-1379
[25] M. Poon et al, *Modelling deuterium release during thermal desorption of D^+-irradiated tungsten,* Journal of Nuclear Materials 374 (2008) 390-402
[26] G.M. Wright et al, *TMAP7 simulations of deuterium trapping in pre-irradiated tungsten exposed to high-flux plasma,* Journal of Nuclear Materials 415 (2011) S636-S640
[27] P. Franzen et al, *Hydrogen trapping in and release from tungsten: Modeling and comparison with graphite with regard to its use as fusion reactor material,* Journal of Nuclear Materials 241-243 (1997) 1082-1086
[28] John R. Taylor, *An Introduction to Error Analysis: The Study of Uncertainties in Physical Measurements,* University Science Books, 1997
[29] P.C. Stangeby, *The Plasma Boundary of Magnetic Fusion Devices,* Taylor & Framcos, 2000
[30] Charlie Spork, *Determination of Hydrogen and Deuterium Inventory of Pre-Treated Targets Using Laser-Induced Desoprtion,* FOM Institute Differ 2013